mathematics

MDPI

Article

Performance and Extreme Conditions Analysis Based on Iterative Modelling Algorithm for Multi-Trailer AGVs

Roberto Sánchez-Martinez [1], J. Enrique Sierra-García [2,*] and Matilde Santos [3,*]

[1] Computer Science Faculty, Universidad Nacional de Educación a Distancia, 28040 Madrid, Spain
[2] Department of Electromechanical Engineering, University of Burgos, 09006 Burgos, Spain
[3] Institute of Knowledge Technology, Complutense University of Madrid, 28040 Madrid, Spain
* Correspondence: jesierra@ubu.es (J.E.S.-G.); msantos@ucm.es (M.S.)

Abstract: Automatic guidance vehicles (AGV) are industrial vehicles that play an important role in the development of smart manufacturing systems and Industry 4.0. To provide these autonomous systems with the flexibility that is required today in these industrial workspaces, AGV computational models are necessary in order to analyze their performance and design efficient planning and control strategies. To address these issues, in this work, the mathematical model and the algorithm that implement a computational control-oriented simulation model of a hybrid tricycle-differential AGV with multi-trailers have been developed. Physical factors, such as wheel-ground interaction and the effect of vertical and lateral loads on its dynamics, have been incorporated into the model. The model has been tested in simulation with two different controllers and three trajectories: a circumference, a square, and an s-shaped curve. Furthermore, it has been used to analyze extreme situations of slipping and capsizing and the influence of the number of trailers on the tracking error and the control effort. This way, the minimum lateral friction coefficient to avoid slipping and the minimum ratio between the lateral and height displacement of the center of gravity to avoid capsizing have been obtained. In addition, the effect of a change in the friction coefficient has also been simulated.

Keywords: mathematical modelling; iterative algorithm; autonomous vehicle; AGV; multi-trailers; simulation; control; Industry 4.0

MSC: 93A30

Citation: Sánchez-Martinez, R.; Sierra-García, J.E.; Santos, M. Performance and Extreme Conditions Analysis Based on Iterative Modelling Algorithm for Multi-Trailer AGVs. *Mathematics* **2022**, *10*, 4783. https://doi.org/10.3390/math10244783

Academic Editors: Ramón Vilanova Arbós and Marian Barbu

Received: 22 November 2022
Accepted: 13 December 2022
Published: 15 December 2022

1. Introduction

In the industrial field, automatic guidance vehicles (AGVs) are frequently used for the transport of specific goods, usually replacing manual means of transport or conveyor belts, in order to reduce operating costs, times, and human errors [1–3]. The irruption of Industry 4.0, the particularization of services, and logistics and flexible production [4], are accelerating the introduction of these AGVs in the industrial sector [5]. On the one hand, these mobile robots increase spatial flexibility, allowing modifications in the location and distribution of production lines in a short time without making changes to the infrastructure. On the other hand, they make it possible to modulate the speed of production and logistics flows to adapt to changes in production planning [6–8]. Even more, as stated in [9], COVID-19 accelerated the demand for online orders, which brought logistics and transportation to the forefront. AGVs were widely used in this context as a part of a reliable and flexible internal transport system. Logistics automation is not restricted to factories or warehouses and can be applied in a wide variety of buildings. Autonomous vehicles can carry raw materials and finished goods in productive centers, such as factories or workshops, and many types of items, such as meals, laundry, or medicines, in hospitals, care homes, or hotels.

There are AGVs with multiple configurations, although the scientific literature seems to focus especially on differential vehicle type, with very little work devoted to the study

of other mobile robots, specifically tricycle type vehicles, widely used in factories and warehouses. This may be due to the greater complexity of vehicles of this type or the hybrid ones, which combine a tricycle-type traction unit and a differential body, especially when studying their dynamics. In addition, multi-trailers are not usually considered in these studies.

However, the need for computational models to study the behavior of these mobile robots and to design efficient and advanced control strategies is undeniable. The use of computer simulation for these vehicles is in line with the assumptions of Industry 4.0. As it is well known, having the chance to test virtual models before real-world application helps to measure the performance, prove the efficiency, identify bottlenecks, study interactions between different system components, experiment and evaluate alternative scenarios, etc. [10,11]. It is necessary to incorporate the dynamics of their behavior in these simulation models to make them realistic and, thus, to be able to test them under critical conditions to guarantee their safety.

For this reason, in this work, first a mathematical model of the dynamics of a hybrid tricycle differential AGV has been developed, and then an iterative algorithm to simulate the movement of this multi-trailer vehicle is implemented. It reflects the dynamics of the drive unit, the AGV body, and the trailers. To do so, the vertical and lateral loads have been considered while studying the static AGV and the AGV in motion, as well as the interaction between the wheels and the ground.

The algorithm has been executed to analyze the influence of the payload, the number of trailers, and the weight distribution, as well as extreme situations of slipping and capsizing. The simulation results are reasonable and allow for improving the efficiency of the designed controls and the safety conditions.

The main contributions of this work can be summarized as follows: Based on the mathematical model, an algorithm to simulate the dynamics of multi-trailer hybrid tricycle differential AGVs has been proposed. The algorithm is hardware independent, as it only receives the traction forces in the wheels as input signals and can be connected to any motor model and controller. Moreover, it has been designed to have low computational complexity, which enables the execution in low-cost industrial controllers. This approach has been used to test complex critical situations in a work environment, such as the risk of overturning, skidding, etc., considering different factors that can lead to these situations. This knowledge can be very useful for the operators of these industrial vehicles. Even more, the use of simulation can provide companies with a significant competitive advantage in the development, implementation, and execution of their plans and manufacturing strategies.

The rest of the manuscript is structured as follows: The state of art and related works are described in Section 2. Section 3 presents a description of the AGV system. In Section 4, the algorithm that implements the model of the dynamics of the vehicle is explained. It presents the three main components of the mobile robot and the interactions between its parts. Vertical and lateral loads and wheel-ground interactions are also considered. The simulation results of critical situations for the AGV are shown and discussed in Section 5. The paper ends with conclusions and future research lines.

2. Related Works

Most of the existing work on the modeling of the dynamics of mobile robots is mainly dedicated to differential robots and vehicles with omnidirectional wheels, given the difficulties presented, in general, by the study of the dynamics of autonomous vehicles [12]. Some exceptions can be found in the literature. Still, the work on the modeling of the dynamics of AGVs is scarce. In the following, we compare the proposals presented by other researchers in comparison to our work in order to highlight the novelty and contributions of this paper. The main differences are mentioned.

Some papers address the tricycle configuration of autonomous robots. For instance, the paper by [13] proposes an approach to modeling a tricycle-type robot using the Euler–Lagrange equations with the aim of designing a non-linear position control law.

Similarly, Yun et al. use the coordinate transformation method and Lagrange equations to establish the kinematics and dynamic model of a three-wheeled mobile robot with two coaxial driving wheels and a driven wheel [14]. Unlike our model, no friction is considered. The validity of the dynamic model of the mobile robot is verified by the path-following simulation of a circular trajectory. Trajectory tracking results showed little deviation from the expected trajectory. No measures of error were given.

In [15], a tricycle collaborative mobile robot (cobot) that can be controlled directly by the operator is modeled with the Euler–Lagrange method. The tricycle cobot has motion with three degrees of freedom (DOF), translations on the plane, and rotation. The motion trajectory is specified based on the given task, but the cobot is moved by a human operator. A laser tracking system is needed to acquire the posture and velocity of the cobot continuously. The performance of the control is evaluated by comparing the planned trajectory and the actual trajectory determined by the simulation model. Straight and circle motions are considered. Errors are obtained in terms of position and orientation.

Unlike these papers, we applied the Newton–Euler approach to obtain the model equations. In general, the Newton–Euler approach provides models with lower computational complexity than Lagrange–Euler. In addition, these works deal with a tricycle configuration AGV instead of a more complex hybrid differential-tricycle one, as in our case.

Another aspect found in the related literature is that most of the papers on AGV models only work with the kinematics of the vehicle and they do not include the possibility of multi-trailer configuration. To mention some, Ref. [16] proposed a mathematical model based on the kinematics in order to predict the behavior of a 2-DOF AGV with differential driving wheels and four caster wheels. The authors concentrated on the estimation of the caster wheels' orientation based only on kinematic means. They do not consider including loads or the slipping or skidding of the wheels. Two simulation scenarios were tested, first was to start turning by a known radius, and the second was to go straight forward after turning, with good predictions of caster wheel orientations.

Models based on data have also been obtained when this information was available. In the case of the paper presented by [17], where different control systems were analyzed for the robust docking maneuvers of an AGV over a predefined route. They used, among others, model-based control techniques that required the development of models of greater or lesser complexity. In the dynamic case, the article described the direction and traction of the AGV; in addition, it modeled the drift phenomena in that direction by means of a transfer function that required identifying the parameters of the real system. Additionally, Suárez et al. used experimental results to obtain models of the direction and longitudinal systems of an autonomous robot [18]. Specifically, the autonomous vehicle is an electrical car, a Citroën Berlingo, with an Ackerman steering system. The models were obtained from the experimental results of several tests conducted on a dedicated circuit. The vehicle is equipped with some instrumentation and control hardware and software. However, in addition to working with no industrial vehicles, on most of the occasions, real data of the vehicle to be modeled are not available, as is our case, and this approach cannot be applied.

Some papers address articulated vehicles with trailers because these robots have some safety issues to be considered. These vehicles exhibit poor maneuverability and low lateral stability compared to heavy trucks and passenger vehicles due to their multi-unit structures, large sizes, and high centers of gravity. Rahimi and He studied active vehicle safety systems for articulated heavy trucks, that is, autonomous cars [19], and more recently, the same authors presented an autonomous driving control strategy for multi-trailer articulated heavy vehicles (MAHV) [20]. A non-linear model predictive control (NLMPC) is designed for direction and speed control of the vehicle. Following these lines, Deng et al. proposed an active linear quadratic regulator (LQR) multi-axle-steering method for MTAHV, but they do not work with AGVs [21]. In [22], the authors address the tracking control problem

of a 16-wheel heavy-duty AGV, whose trajectory is based on magnetic navigation sensors. The vehicle model is simplified to a two-wheel AGV model. A trajectory tracking fuzzy control for circular/straight trajectories is simulated with MATLAB/Simulink to verify the effectiveness of the trajectory control.

A similar approach is presented in [23,24] to improve both, the maneuverability and stability of articulated heavy vehicles. To tackle this conflicting design problem, a closed-loop dynamic simulation-based design method of these vehicles with active trailer steering systems is developed. In order to evaluate vehicle performance under a well-defined testing maneuver, a driver model is introduced, so the vehicle model follows a prescribed route at a given speed. In the second paper, the authors change the optimization method to one with a lower computational cost and a parallel computation technique with a master-slave system.

Different multi-trailer systems (MTS) were described and studied in Govender's doctoral thesis, but within a port terminal environment and thus focused on the transportation of multiple containers using a single tractor [25]. Similarly, in the paper by Ottjes et al., a generic object-oriented simulation model for overland transport of containers is presented [26]. Three types of transportation vehicles are considered for handling containers: automated guiding vehicles, automated lifting vehicles, and the multi-trailer system with manned traction units. The container flow is simulated in the Rotterdam Port.

Veiga et al. proposed the dynamic modeling of an AGV in [27]. Two models of a towing car system with three linked towed cars are compared. A simplified version of a complete multi-body model of one system is proposed. The second model was developed in Modelica and resulted in a more stable in order to estimate the relative trajectories between the vehicles and the maximum allowed speed when taking a curve without capsizing or sliding.

Jodejko-Pietruczuk and Werbińska-Wojciechowska address the reliability and maintenance issues of a multi-AGV system developing a Monte Carlo simulation model [28] The work by Sasamoto et al. overviews the modeling, implementation, and mechanical characterization of a differential-drive mobile robot configuration for which the mathematical model was obtained [29]. Such a model allows the simulation of the AGV's motion and can be used to improve productivity, increase automation, and reduce transportation costs in industrial facilities. In addition, a prototype of the AGV was built.

An interesting work on AGV modeling is proposed by Smieszek et al., where the different errors that occur in an AGV whose only way of knowing its position is by means of odometry are obtained [30]. It focuses on studying the effect of load distribution on the effective radius of the wheels and, therefore, on the trajectory followed by the AGV. In addition, it is shown that the variation of the effective radius of the wheel also influences the knowledge of the actual distance between points on contact of the wheels.

Finally, a recent interesting literature review on AGV control has been published by Reis et al. As it states, both classical control and artificial intelligence-based techniques were primarily used in kinematic controllers [31]. The four topics addressed in this paper are: the control strategies used in the AGV position control problem, how the literature presents the AGV operating requirement of position accuracy, how the literature validates the proposed controller and presents their results regarding the system's position accuracy, and the technological tendencies the proposed solutions reveal. The implementation of a kinematic control strategy in a programmable logic controller (PLC) is shown in Molledo [32]. In order to improve the fine-tuning of the controller, in this work, an IEC61131-based simulation tool has been developed to evaluate the performance of the controller with different trajectories in terms of minimum guide error. The tool can run on a computer or on the AGV's PLC. Moshayedi et al. present the modeling and simulation of dual-wheeled differential AGV systems equipped with an array of 16 magnetic sensors accompanying the PID controller [33]. The main parts of the AGV, i.e., the body, engine and driver, processor, and sensors, are described. Then, a PID controller is adjusted with different methods, including evolutionary optimization. It was tested on a real low-scale model of the mobile robot on several paths with different shapes. Additionally, based on the kinematic model in [34], a

camera sensor is used to measure the tracking position error and heading angle error of a tricycle-wheeled mobile robot with three wheels. Based on these errors, a controller that integrates two control loops, an inner loop and an outer loop, is designed for this AGV. The outer loop control is based on a fuzzy logic framework, and the inner loop control is based on two conventional PID controllers.

To summarize, previous works on multi-trailer AGVs are scarce in the literature, and to the best of our knowledge, there are no other works on the modeling of the dynamics of these systems using a Newton–Euler approach and the consideration of extreme conditions. Other differences that may be worth it to remark are the following. The mentioned papers do not deal with hybrid configurations of AGVs, but rather differential ones (most of them) or only tricycle ones. They are mainly focused on the kinematics of autonomous vehicles. Some of them work with very different types of vehicles (cars, tractors, etc.). The models are oriented toward control or safety issues, and in some cases, they are based on data. They work with different sensors. Thus, on the one hand, this makes it difficult to compare the quantitative results with other proposals, and, on the other hand, you can say that the dynamic model of the multi-trailer hybrid tricycle differential AGV here proposed is novel and original.

3. Multi-Trailer AGV Description

Depending on how the loads are transported, AGVs can be classified into several categories, such as: tow AGVs, platform AGVs, and automated forklifts. Automated forklifts are used to pick and place loads at different heights. Platform AGVs, also called turtles, transport the loads on top of them. Indeed, the weight of the payload increases the total weight, and in some cases, this fact is used to ensure the grip and prevent the AGV from skidding. In this type of vehicle, as the weight of the load is fully supported by the AGV, very high-performance motors are required, as they are normally used to move loads below 2 tons. However, specific and ad-hoc AGVs are built to move bigger loads, such as in the aeronautic or wind energy sectors.

To alleviate the torque demand of the motors, make smaller AGVs feasible, and reduce the cost of the automated logistic solutions, two AGVs were used. In this type of vehicle, the load is transported in a cart or trailer, so the payload is towed rather than supported. The weight of the payload falls on the wheels of the trailer. Usually, the trailers have four wheels, with two rigid wheels and two swivel wheels. Depending on the application, it is common to find several trailers, as shown in Figure 1. To study these complex systems, it is important to have multi-trailer AGV mathematical models available and be able to simulate them.

Figure 1. Example of multi-trailer AGV [35].

Figure 2 shows a schematic representation of a multi-trailer AGV. The AGV is the rectangle in blue, and the trailers are the rectangles in red. Each trailer has two points marked; the black circle denotes the point used to locate the position of the trailer and the

red circle indicates the location of the center of gravity. The position of each trailer is taken from the center of its rear axle.

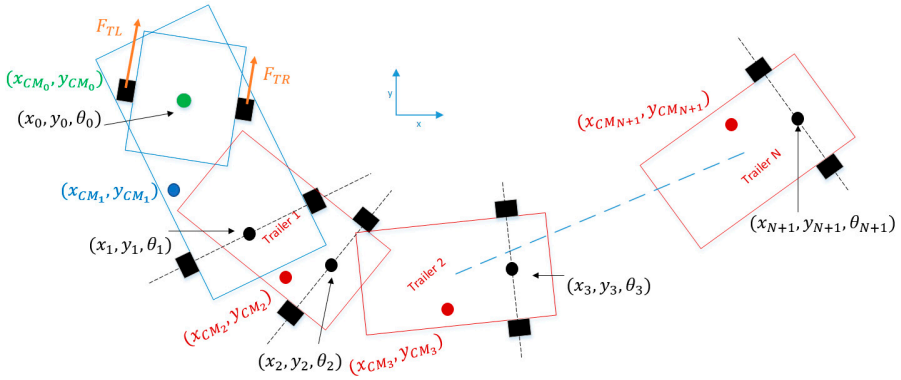

Figure 2. Multi-trailer AGV schematic representation.

The kinematic model of the two AGVs is normally based on a differential robot or a tricycle one. In our case, to make the approach more general, we have used a hybrid AGV that combines both. That is, the traction unit moves similar to a differential robot, whose center is given by coordinates $(x_0,\ y_0,\ \theta_0)$ (see Figure 2, blue rectangle), where x_0 and y_0, are the x-axis and y-axis coordinates, and θ_0 is the orientation in the inertial frame. This unit is linked to the body of the AGV and rotates around a pivot shaft (green circle, Figure 2). The center of gravity has been located at the center of the traction unit as this is the standard approach, thus $(x_0,\ y_0)$ matches with $(x_{CM_0},\ y_{CM_0})$. The traction unit acts as the steering wheel in a tricycle, and so the body of the AGV moves similar to a tricycle robot.

The position of the AGV is given by $(x_1,\ y_1,\ \theta_1)$ and the location of its center of mass in the inertial frame by $(x_{CM_1},\ y_{CM_1})$. Additionally, it may be observed in Figure 2 that the position of the i-trailer is represented by $(x_{i+1},\ y_{i+1},\ \theta_{i+1})$, and its center of gravity by $(x_{CM_{i+1}},\ y_{CM_{i+1}})$. As the vehicle may have N trailers, the position of the last trailer is given by $(x_{N+1},\ y_{N+1},\ \theta_{N+1})$.

The system moves as a result of two external forces, F_{TL} and F_{TR}. The controller of the system adjusts these forces to make the AGV follow the desired path. The control architecture is shown in Figure 3. Normally, these forces are the result of the torques exerted by the motors; however, we have used these forces as inputs to the system to obtain a more general approach.

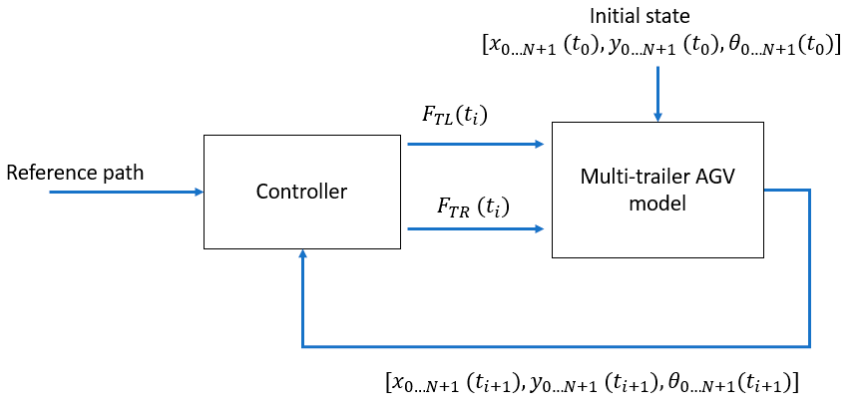

Figure 3. Multi-trailer AGV model and control interaction architecture.

In this work, we focus on the development of an algorithm that implements the multi-trailer AGV model (Figure 3, right side). This way, it can be used with any control strategy. However, a basic controller has been used to validate the modeling approach in the simulation.

4. Multi-Trailer AGV Modelling Iterative Algorithm

The modeling algorithm can be run in open-loop or in closed-loop with a controller. In an open-loop scheme, the model of the multi-trailer AGV shows the evolution of the state of the AGV and the trailers, $[x_{0\ldots N+1}\ (t_i),\ y_{0\ldots N+1}\ (t_i),\ \theta_{0\ldots N+1}(t_i)]$ in $t_i \in \{t_1, t_2, \ldots, T_{sim}\}$, given a set of initial states $[x_{0\ldots N+1}\ (t_0),\ y_{0\ldots N+1}\ (t_0),\ \theta_{0\ldots N+1}(t_0)]$ and the application of the external forces $[F_{TL}\ (t_i),\ F_{Tr}\ (t_i)]$ in $t_i \in \{t_1, t_2, \ldots, T_{sim}\}$.

In the closed-loop scheme, the objective of the multi-trailer AGV modeling iterative algorithm is to calculate the new state of the AGV and the trailers $[x_{0\ldots N+1}\ (t_i),\ y_{0\ldots N+1}\ (t_i),\ \theta_{0\ldots N+1}(t_i)]$ given the past state of the AGV and trailers, $[x_{0\ldots N+1}\ (t_{i-1}),\ y_{0\ldots N+1}\ (t_{i-1}),\ \theta_{0\ldots N+1}(t_{i-1})]$, and the application of a pair of external forces, $[F_{TL}\ (t_i),\ F_{Tr}\ (t_i)]$, obtained by the controller. The controller receives this new state and calculates the new forces, $[F_{TL}\ (t_{i+1}),\ F_{Tr}\ (t_{i+1})]$. This process is iteratively performed during the simulation time $t_i \in \{t_1, t_2, \ldots, T_{sim}\}$.

Before presenting the modeling algorithm, some of the steps are detailed below.

Initialization of the algorithm:

- The mass of the AGV and the trailers is known and is given by m_{AGV_i} for $i \in 1 \ldots N+1$.
- The inertia of the traction unit is known and is given by I_{DU}. The inertia of the AGV body and the trailers are known and are given by I_{AGVi} for $i \in 1 \ldots N+1$.
- The position and orientation of the AGV and the trailers in the inertial frame are known and are given by $(x_{0\ldots N+1},\ y_{0\ldots N+1},\ \theta_{0\ldots N+1})$.

Before presenting the modelling algorithm, some of the steps are detailed below.

- The velocity of the AGV and the trailers in the inertial frame are known and given by $\left(\dot{x}_{0\ldots N+1},\ \dot{y}_{0\ldots N+1},\ \dot{\theta}_{0\ldots N+1}\right)$.
- The center of mass of the AGV and the trailers in the inertial frame are known and given by $\left(x_{CM_{0\ldots N+1}},\ y_{CM_{0\ldots N+1}}\right)$.

Stop conditions:

- The AGV or any of the trailer's skid, i.e., $sk_i \neq 0\ i \in 1 \ldots N+1$.
- The AGV or any of the trailer's capsizes, i.e., $cap_i \neq 0\ i \in 1 \ldots N+1$.
- The simulation ending time T_{sim} is reached.

Simulation process:

The algorithm performs the following calculations at each simulation step:

1. Calculation of the traction force and acceleration of the assembly from the total mass and the torques applied to the wheels. The AGV or any of the trailer's capsizes, i.e., $cap_i \neq 0\ i \in 1 \ldots N+1$.
2. Calculation of the turning radius of the AGV.
3. Calculation of the centrifugal force in the AGV.
4. Calculation of the lateral forces on the wheels considering interactions between components.
5. Calculation of the vertical loads on the wheels, considering the interactions between different components. For example, the body of the AGV unloads much of its weight on the traction unit and, in turn, the trailers can unload some of their weight on the previous component.
6. Calculation of the slip from the vertical and lateral loads on each wheel.
7. Correction of the direction of application of the tractive force based on the calculated slip.
8. Verification that none of the components is in a capsizing or skidding situation.
9. For each trailer of the system:
    a. Calculation of the direction of the tractive force that is the direction of the displacement of the previous component (trailer or AGV).
    b. Calculation of the vertical and lateral forces, and the slip.
    c. Correction of the direction of application of the tractive force based on the calculated slip for the wheels of the specific component.
    d. Calculation of the acceleration of the CM as a function of the tractive force and the mass of the whole assembly.

e. Integration of acceleration to obtain velocity.
f. Integration of the velocity to obtain the position of the CM.

This process is formalized by Algorithm 1, showing how some of the equations of the mathematical model are implemented.

Algorithm 1. Multi-trailer AGV iterative modelling algorithm.

$m_t \leftarrow CalculateTotalMass(m_0, \ldots, m_{N+1})$
$t = t_0$
While $\{t < T_{sim}\} \wedge \forall_i \{sk_i = 0\} \wedge \forall_i \{cap_i = 0\}$ {
$F_{TR}, F_{TL} \leftarrow Controller(\dot{X}_0, v_d, x_0, y_0, \theta_0, path)$
$F_T \leftarrow F_{TR} + F_{TL}$
$M_0 \leftarrow (F_{TR} - F_{TL})/(2y_0)$
$\ddot{\beta} \leftarrow M_0/I_0$
$\ddot{X}_0 \leftarrow F_T/m_T$
$R_1 \leftarrow CalculateRTurn(\beta)$
$F_{C,1} \leftarrow m_1 \cdot \dot{X}_1 \cdot \dot{X}_1/R_1$
$[F_{yF,1} \quad F_{yR,1}]^T \leftarrow CalculateYForce(F_{C,1}, F_T, \beta, x_{CM,1})$
$[F_{zF,1} \quad F_{zR,1}]^T \leftarrow CalculateZForce(m_1, x_{CM,1}, X_1, g)$
$[s_{yF,1} \quad s_{yR,1}]^T \leftarrow CalculateYSlip(F_{Z,1}, F_{Y,1}, k_y)$
$\beta \leftarrow ApplySlip(\beta, s_{yF,i}, s_{yR,i})$
$\ddot{\theta}_1 \leftarrow 1/I_1 \cdot (F_T \cos(\dot{\beta}) \cdot y_{CM,1} + F_T \sin(\dot{\beta}) \cdot (\mathrm{x_{CM,1}} - x_{CT,1}))$
$[\dot{x}_1 \quad \dot{y}_1]^T \leftarrow \dot{X}_0 \cdot \cos(\beta) \cdot [\cos(\theta_1) \quad \sin(\theta_1)]^T$
$[x_1 \quad y_1]^T \leftarrow \int [\dot{x}_1 \quad \dot{y}_1]^T$
$\beta \leftarrow \int \dot{\beta}$
$\dot{\beta} \leftarrow \int \ddot{\beta}$
$\theta_1 \leftarrow \int \dot{\theta}_1$
$\dot{\theta}_1 \leftarrow \int \ddot{\theta}_1$
$cap_1 = CalculateCapzizing(R_1, \dot{X}_1)$
$sk_1 = CalculateSkipping(R_1, \dot{X}_1)$
For $i = 2$ to $N + 1$ {
$\gamma_i \leftarrow \theta_{i-1} - \theta_i$
$R_i \leftarrow CalculateRTurn(\gamma_i)$
$F_{C,i} \leftarrow m_i \cdot \dot{X}_i \cdot \dot{X}_i/R_i$
$[F_{yF,i} \quad F_{yR,i}]^T \leftarrow CalculateYForce(F_{C,1}, F_T, \beta, x_{CM,1})$
$[F_{zF,i} \quad F_{zR,i}]^T \leftarrow CalculateZForce(m_t, x_{CM,i}, x_i, g)$
$[s_{yF,i} \quad s_{yR,i}]^T \leftarrow CalculateYSlip(F_{Z,i}, F_{Y,i}, k_y)$
$\gamma_i \leftarrow ApplySlip(\gamma_i, s_{yF,i}, s_{yR,i})$
$\ddot{\theta}_i \leftarrow 1/I_i \cdot (F_T \cos(\dot{\gamma}_i) \cdot y_{CM,i} + F_T \sin(\dot{\gamma}_i) \cdot (\mathrm{x_{CM,i}} - x_{CT,i}))$
$[\dot{x}_i \quad \dot{y}_i]^T \leftarrow \leftarrow \dot{X}_0 \cdot \cos(\dot{\gamma}_i) \cdot [\cos(\theta_i) \quad \sin(\theta_i)]^T$
$[x_i \quad y_i]^T \leftarrow \int [\dot{x}_i \quad \dot{y}_i]^T$
$\theta_i \leftarrow \int \dot{\theta}_i$
$\dot{\theta}_i \leftarrow \int \ddot{\theta}_i$
$cap_i = CalculateCapzizing(R_i, \dot{X}_i)$
$sk_i = CalculateSkipping(R_i, \dot{X}_i)$
}endFor
$t = t + \Delta T$
}endWhile

Therefore, the first step is the calculation of the position of the center of mass of each trailer and the AGV body. The algorithm then calculates the global acceleration of the AGV and the angular acceleration of the drive unit. Then, a similar calculation is carried out for the AGV body, which is referred to in the algorithm as AGV1. That is, calculations for the trailers are performed in a loop in the same way as for the AGV body. In the case of working with a stationary load, the CM position can be obtained outside the simulation since it will remain constant. This is based on the overlapping principle, which is applicable since all the simulated components are linear.

The equations of Algorithm 1 are software-independent, and could be implemented in any programming language, as no specific library is required. Additionally, the equations involved only use simple arithmetic operations, such as additions, multiplications, divisions, and standard trigonometric functions; so, they have low computational complexity. A typical control time for AGV applications is 10 ms. Therefore, these equations can be run on low-cost hardware devices and standard PLCs.

To facilitate the implementation, the inputs and outputs of the algorithm, as well as the variables involved with the corresponding units, are summarized in Table 1.

Table 1. Inputs and outputs of the algorithm.

Input		Output	
Name	**Description**	**Name**	**Description**
m_i	AGV (traction unit, body or, trailer) mass in kg.	M_0	Turning torque applied to the drive unit in Nm.
CM_i	AGV (body or trailer) center of mass coordinates (x, y, z) in m.	$x_0,\ y_0, x_1,\ y_1, x_i,\ y_i$	Drive unit, AGV, and trailer position respect to the fixed reference frame in m.
$F_{TR},\ F_{TL}$	Right and left longitudinal traction forces in N	β	Angle between drive unit and AGV body in rad.
$X_0,\ Y_0, X_1,\ Y_1, X_i,\ Y_i$	Drive unit, AGV or trailer x and y coordinates referred to their own reference frame in m.	θ_i	Angle between the component i body and fixed reference frame in rad.
g	Gravity (m/s^2)	$s_{yF,i},\ s_{yR,i}$	Lateral slip in the front (f) and rear (r) axles in the i-component.
k_v	Lateral slip coefficient.	F_C	Centrifugal force in N.
$I_0,\ I_0, I_i$	Drive unit, AGV and trailer inertia in kgm^3	$F_{zF,i},\ F_{zR,i}$	Lateral force in the front (f) and rear (r) axles in the i-component in N.
$F_{yF,i},\ F_{yR,i}$	Lateral force in the front (f) and rear I axles in the i-component in N.	R_i	Turning radius of the i-component in m.

As with any physical system, this model is subject to uncertainties and disturbances. Thus, to design effective control strategies, it is important to consider them. The most relevant ones have been summarized in Table 2. We have classified them, considering whether the uncertainty comes from the AGV, the application, or the environment. Furthermore, we have recommended a way to include this uncertainty source in the model.

The mathematical equations of the model that are implemented in the algorithm are further explained in the following sections. Section 4.1 proposes different control implementation approaches. The dynamic model of each of the components of the AGV will be developed, that is, the drive unit (Section 4.2), the body (Section 4.3), and the trailer (Section 4.4). Finally, to complete the dynamics equations of the AGV, the loads on the wheels (Sections 4.5 and 4.6) and the wheel-ground interaction (Section 4.7) will be calculated.

Table 2. Uncertainty sources in the model.

Uncertainty Source	Source Type	Description	Modelling Recommendation
Payload of the AGV	Application	In some applications, the payload is variable and unknown.	Can be modeled as a train of pulses with variable amplitude.
Payload of each trailer	Application	In some applications, the payload is variable and unknown.	Can be modeled as a train of pulses with variable amplitude.
Ground friction	Environment	The friction normally is unknown, and it varies with the location and time.	Can be modeled as a function of the location f(x,y). This function can be smooth or with discontinuities.
Noise in the guiding sensor	AGV/environment	The guiding sensor is affected by electrical noise. It is mainly caused by the effect of the motors and defects in the guiding tapes or landmarks.	Can be modeled as white Gaussian noise or other noise types.
Noise in the speed sensor	AGV	The speed sensors are affected by electrical noise. It is mainly caused by the effect of the motors.	Can be modeled as white Gaussian noise or other noise types.
Friction in the axles	AGV/environment	Dry and viscous friction are applied in the axles. The friction coefficients can be initially known; however, they can change during the working operation as an effect of degradation. In addition, some object could suddenly block the wheels producing a jump in the friction.	These coefficients can be modeled as ramps with very small negative slopes. In addition, a step can be used to simulate that wheels are partially blocked with some object.
Radius of the wheels	AGV/environment	The wheels degrade with the time and the radius decreases during the lifespan.	Can be modeled as a ramp with a very small negative slope. Each wheel degrades at a different speed.

4.1. Control Implementation Example

The proposed algorithm is hardware independent, as it receives the input force signals from a generic controller. The implementation of this controller can be based on any control technique. However, to evaluate the proposed model of the AGV, we used a control strategy based on two PIDs with saturated outputs. The first PID is used to obtain the traction effort F_T that is necessary to achieve the target speed. The second PID applies a delta ΔF_T to the calculated traction force, based on the guiding error err_{gui}, in order to generate a rotating torque at the center of the traction unit. The guiding error is obtained by a guiding sensor and can be simulated as detailed in [36].

The implementation of the application of this controller to the AGV is detailed in Algorithm 2. The last two lines correspond to the saturation of the control action.

Figure 4 shows a control scheme for the implementation of Algorithm 2. It is possible to observe that the multi-trailer AGV receives the references for the traction forces of the left and right wheels, F_{TL} and F_{TR}. The guiding sensor calculates the guiding error, err_{gui}, considering the location of the AGV and the path. This signal is used by the trajectory PID control to generate the reference ΔF_T. On the other hand, the speed of the AGV, v_d feeds the speed PID controller which obtains the signal F_T. Both signals, F_T and ΔF_T are used to calculate the references for the wheels, F_{TL} and F_{TR}.

Algorithm 2. Simple PID controller to test the modelling approach.

$$
\begin{aligned}
&F_{TR},\ F_{TL} \leftarrow Controller\left(\dot{X}_0, v_d,\ x_0, y_0, \theta_0, path\right)\\
&\quad err_v \leftarrow \dot{X}_0 - v_d\\
&\quad err_{gui} \leftarrow sensor(x_0, y_0, \theta_0, path)\\
&\quad F_T \leftarrow K_{P,v}{\cdot}err_v + K_{D,v}{\cdot}\dot{err}_v + K_{I,v}{\cdot}\int err_v\\
&\quad \Delta F_T \leftarrow K_P{\cdot}err_{gui} + K_D{\cdot}err_{gui} + K_I{\cdot}\int err_{gui}\\
&\quad F_{TR} \leftarrow \max\left(\min(F_T + \Delta F_T, F_{T,max}), F_{T,min}\right)\\
&\quad F_{TL} \leftarrow \max\left(\min(F_T - \Delta F_T, F_{T,max}), F_{T,min}\right)
\end{aligned}
$$

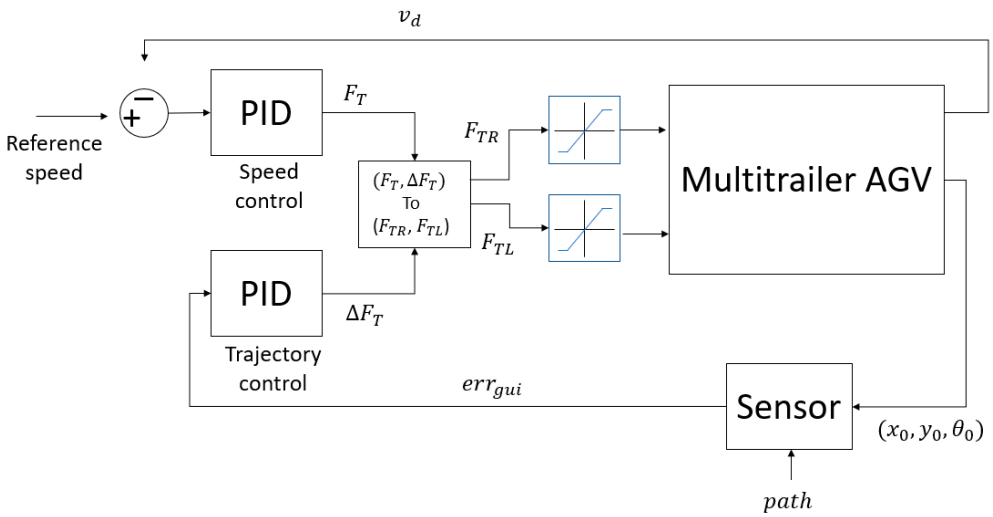

Figure 4. Double PID control scheme.

In Figure 5, the speed PID controller is substituted by a fuzzy logic controller (FLC). It receives the speed error and its derivative as inputs and obtains the signal F_T as output. The rest of the scheme is the same as in Figure 4. The speed control must face uncertainties and disturbances, such as changing payloads, unknown frictions, etc.; hence, it may be interesting to use a fuzzy control to tackle these issues.

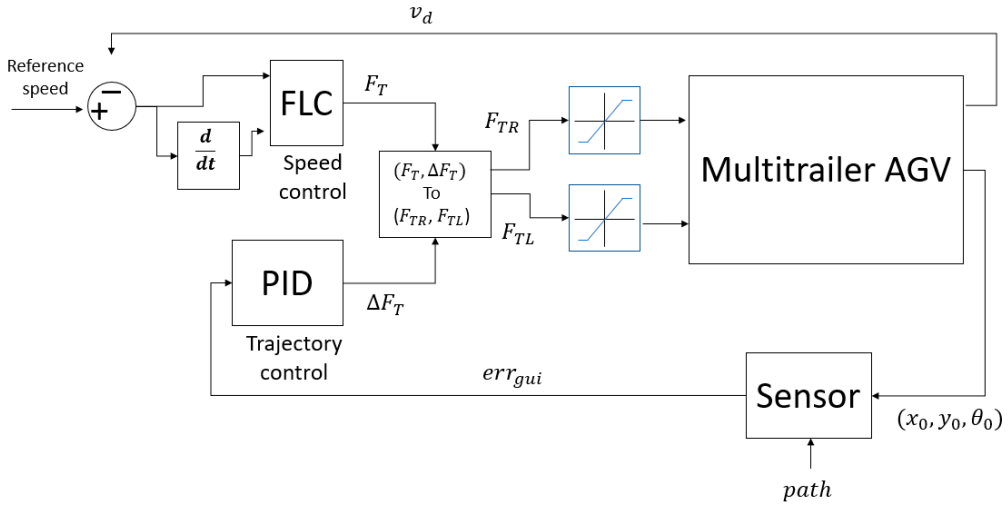

Figure 5. PID and Fuzzy Logic Control scheme.

4.2. Drive Unit Dynamics Model

From a modeling point of view, the drive unit is affected by the load distribution in terms of normal forces, which affect each of the wheels. The traction unit generates a traction force that is applied to a fixed point of the AGV body, called the pivot shaft point (CT), which matches the center of mass of the traction unit (CM). This is a common assumption, as the traction units of these hybrid AGVs are normally symmetric. Anyway, it would be possible to adapt the equations to locate the CM at any other point.

Figure 6 shows the forces applied to the traction unit. As it can be seen, the forces applied to the wheels cause a movement of the traction unit in the x-direction of the coordinate system and a rotation around the CT.

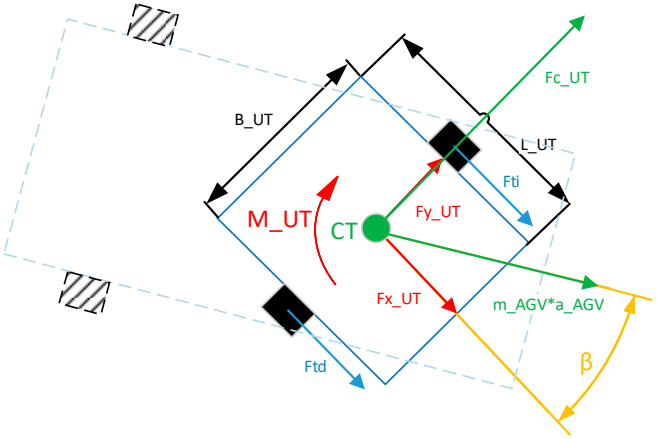

Figure 6. Model of the traction unit.

Applying the Newton–Euler method, the following equations are obtained for this component of the AGV.

$$\begin{bmatrix} m_{AGV} & 0 & 0 \\ 0 & m_{AGV} & 0 \\ 0 & 0 & I_{UT} \end{bmatrix} \ddot{q} = \begin{bmatrix} (F_{TR} + F_{TL}) + m_{AGV} * a_{AGV} * cos(\beta) \\ F_{cUT} + m_{AGV} * a_{AGV} * sin(\beta) \\ \frac{F_{TL} - F_{TR}}{B_{UT}} \end{bmatrix} \quad (1)$$

$$q = \begin{bmatrix} x_{UT} \\ y_{UT} \\ \beta \end{bmatrix} \quad (2)$$

where parameters are defined in Abbreviations section at the end of the article.

It is appropriate to note that x_{UT} and y_{UT} are denoted in Figure 1 and in Algorithm 1 as x_0 and y_0, Assuming the non-slip situation, the traction unit is forced not to move in the y-axis direction, therefore:

$$\ddot{y}_{UT} = 0 \rightarrow F_{cUT} = -F_{yUT} \quad (3)$$

In addition, the traction unit cannot be separated from the body of the AGV, so the relative speed between them is zero, as shown in the following:

$$\ddot{x}_{UT} = 0 \rightarrow F_{xUT} = -(F_{TR} + F_{TL}) - m_{AGV} * a_{AGV} * cos(\beta) \quad (4)$$

The centrifugal force is expressed by the following equation:

$$F_C = \frac{m_{AGV} V^2}{R_{turn}} \quad (5)$$

The radius of the curve can be calculated as:

$$R_{turn} = L_E * ctan(\beta) \tag{6}$$

where L_E is the distance between the center of the rear axle and the center of the traction unit.

4.3. Model of the AGV Body Dynamics

To model the AGV as a tricycle, we consider that the traction unit acts with a force *Ft* over the body of the AGV. To define the equations of the AGV body dynamics, four significant points can be differentiated (Figure 7).

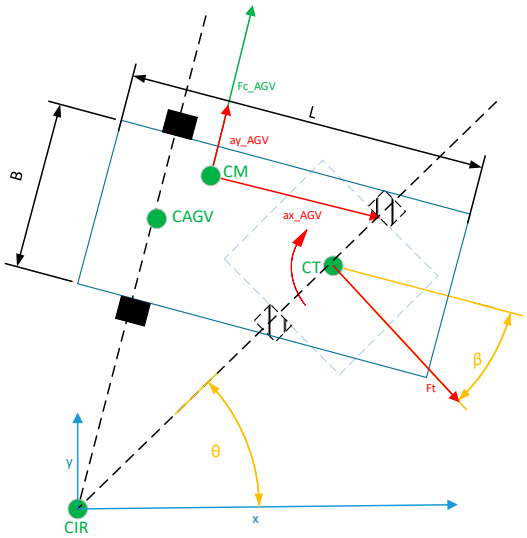

Figure 7. Model of the body of the AGV.

1. The drive unit center, CT.
2. The center of the AGV, called the CAGV, is located in the middle of the axle that connects the rear wheels.
3. The center of mass, CM, influences the moment of inertia of the AGV.
4. The instantaneous center of rotation, CIR, is the point about which the AGV rotates as a whole.

Then, by applying the Newton–Euler method on the CM of the AGV, the following equations are obtained:

$$\begin{bmatrix} m_{AGV} & 0 & 0 \\ 0 & m_{AGV} & 0 \\ 0 & 0 & I_{AGV_1} \end{bmatrix} \ddot{q} = \begin{bmatrix} F_t * \cos(\beta) \\ F_{cAGV} + F_y - F_t * \sin(\beta) \\ F_t \cos(\beta) y_{CM} + F_t \sin(\beta) * (x_{CM} - x_{CT}) \end{bmatrix} \tag{7}$$

$$q = \begin{bmatrix} x_{CM_{AGV}} \\ y_{CM_{AGV}} \\ \theta_1 \end{bmatrix} \tag{8}$$

It is appropriate to note that $x_{CM_{AGV}}$ and $y_{CM_{AGV}}$ are denoted in Figure 1 and in Algorithm 1 as x_{CM_1} and y_{CM_1}, Again, due to the non-slip hypothesis, the body of the AGV is forced not to move in the direction of the y-axis, hence we can express it as:

$$\ddot{y}_{AGV1} = 0 \ \rightarrow F_{cAGV} + F_y = F_t * \sin(\beta) \tag{9}$$

4.4. Trailer Dynamics

To simulate the trailer, it can be considered similar to a tricycle-type AGV, whose "traction unit" would apply a traction force at the center of the trailer (CR). Following this approach, the Euler–Newton method has been applied to this subsystem, and all forces acting on the trailer have been identified. A two-wheeled trailer has been chosen as representative of those most used in industrial robotics. Although the trailer has four wheels, only the two rigid wheels are shown in Figure 8, as the other two swivel wheels at the front of the trailer rotate freely, and hence, they do not introduce any additional kinematic constraints. For the purposes of this work, it is assumed that these swivel wheels do not affect the AGV dynamics, and thus no additional torque is required to align these wheels during direction changes.

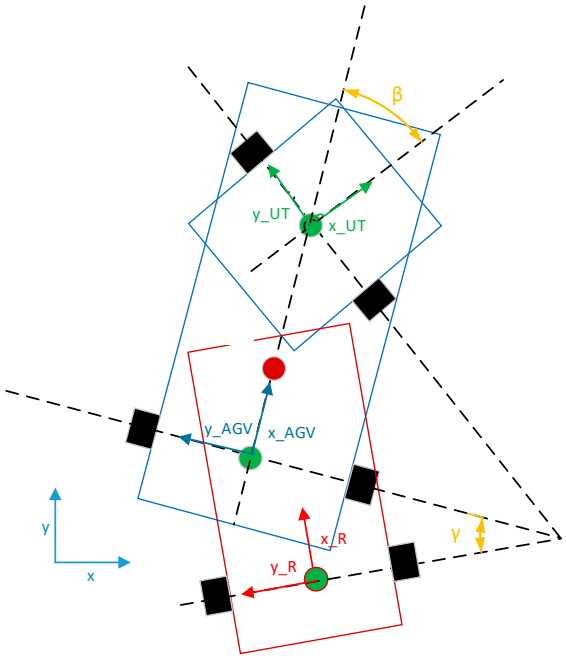

Figure 8. AGV and Trailer scheme.

Figure 8 shows, schematically, the AGV and trailer assembly. In this case, a fourth reference system must be added to the trailer [x_R, y_R] (Figure 8). The relationship between these coordinate systems is represented in Figure 9.

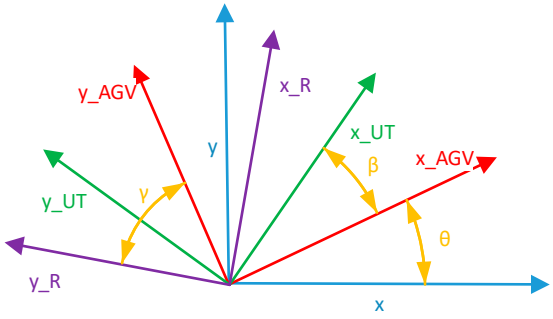

Figure 9. Reference system with trailer.

The forces (green lines) applied to the trailer are represented in Figure 10.

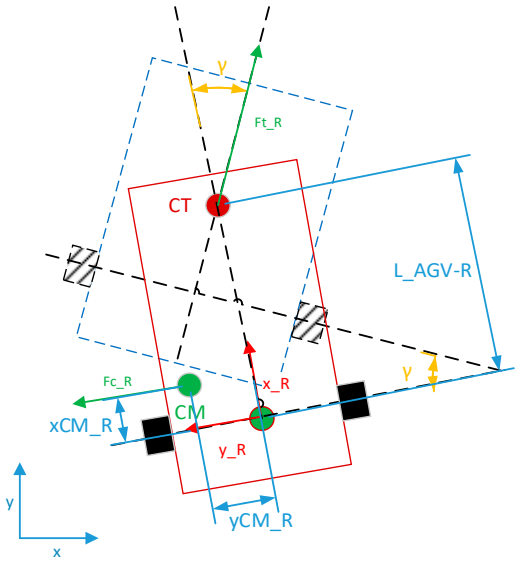

Figure 10. Forces acting on the trailer.

The application of the balance of forces in CM and the balance of torques in CR can be expressed as Equation (10)–(12).

$$F_{cR} * (L_{AGV-R} - x_{CM}) = I_R \ddot{\gamma} \tag{10}$$

$$F_t \cos(\gamma) = m_R \ddot{x}_{CM_R} \tag{11}$$

$$F_{tR} \sin(\gamma) + F_{cR} = m_R \ddot{y}_{CM_R} \tag{12}$$

Putting them in matrix form and generalizing,

$$\begin{bmatrix} m_R & 0 & 0 \\ 0 & m_R & 0 \\ 0 & 0 & I_R \end{bmatrix} \ddot{q} = \begin{bmatrix} F_t \cos(\gamma) \\ F_{tR} \sin(\gamma) + F_y + F_{cR} \\ F_{cR} * \left(L_{AGV-R} - x_{CM_R}\right) \end{bmatrix} \tag{13}$$

$$q = \begin{bmatrix} x_{CM_R} \\ y_{CM_R} \\ \gamma \end{bmatrix} \tag{14}$$

The addition of the trailer affects the vertical load distribution of the AGV as the weight of the trailer is distributed between the body of the AGV (towing center) and the trailer wheels. Therefore, the total center of mass of the system changes its position when adding the trailer.

Applying the no-slip hypothesis, the trailer is forced not to move in the direction of the y-axis, that is:

$$\ddot{y}_{CM_R} = 0 \ \rightarrow F_{cR} + F_y = -F_{tR} * \sin(\gamma) \tag{15}$$

In addition, the centrifugal force of the AGV is assumed to be fully compensated by the AGV wheels without affecting the trailer.

4.5. Vertical Loads on Wheels

The relevance of knowing the loads supported by the wheels appears when including the interaction between the wheels and the ground in the dynamic model, since most of the existing models in the literature (magic formula, etc.) use both loads to calculate the wheel slip on a running surface. To calculate the load on each wheel, it is necessary to apply a balance of forces and moments in each of the three planes, despite the fact that the AGV only moves in the XY plane. For convenience, two cases will be distinguished to calculate the vertical loads:

1. Static AGV: No tensile forces or momentums. The AGV and its load are resting on the surface. The only forces that are exerted by the weight of the loads are the AGV and trailers. The objective of this section is to calculate for each trailer the position of its center of mass.
2. AGV in motion: There are pulling momentum and forces as the AGV is moving. In addition, centrifugal force can also appear when turning. However, the weight is not considered in this case as it is taken into account in the static case.

Since we are dealing with a linear system, we can apply the superposition principle and decouple the static forces from the dynamic ones. This allows simulation calculations to be simplified and memory and processor time to be saved.

4.5.1. Static AGV

In this case, we consider an AGV transporting several packages whose masses and centers of mass are known. The mass and the position of the center of mass of the AGV are also known. Figure 11 represents a possible schema for this scenario. The same approach is valid and can be applied for each trailer.

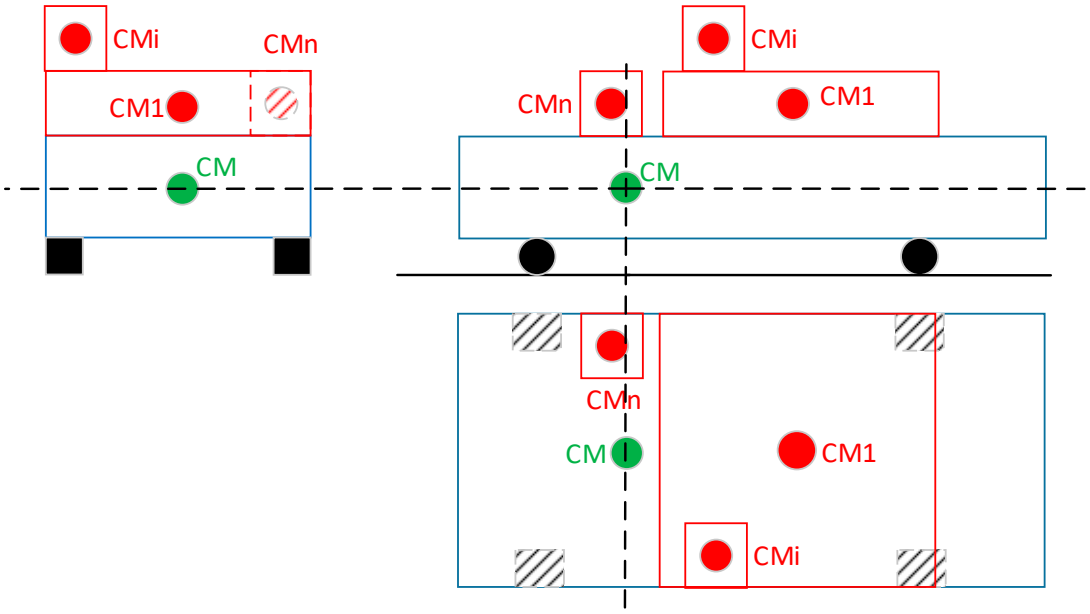

Figure 11. AGV diagram to obtain the position of the AGV center of mass.

Applying the balance of forces and moments around the CM of the AGV, the equations to calculate the displacement of the center of mass are obtained, (16)–(18).

$$d_x = \frac{1}{m_{AGV} + \sum_{i=1}^{n} m_i} \sum_{i=1}^{n} m_i x_i \tag{16}$$

$$d_y = \frac{1}{m_{AGV} + \sum_{i=1}^{n} m_i} \sum_{i=1}^{n} m_i y_i \tag{17}$$

$$d_z = \frac{1}{m_{AGV} + \sum_{i=1}^{n} m_i} \sum_{i=1}^{n} m_i x_z \tag{18}$$

In Figure 12, the view from above the AGV with the position of the center of mass is represented. Since we are considering the static case and there are no forces in the x and y axes, it is not necessary to render views that include the height. In this case, everything has been arbitrarily referenced to the geometric center of the AGV.

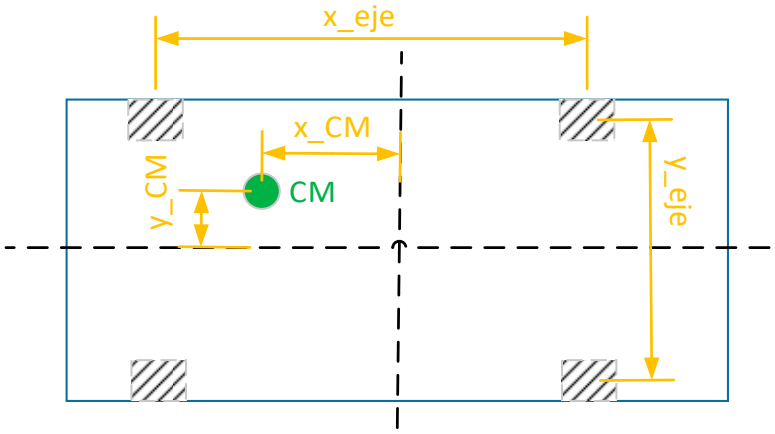

Figure 12. AGV top view. Position of the resulting center of mass.

Applying the balance of forces and moments with respect to the geometric center; the resulting equations are:

$$\sum F_z = m_{t-AGV} * g \tag{19}$$

$$(F_{zB} - F_{zF})\frac{x_{eje}}{2} = m_{t-AGV} * g * x_{CM} \tag{20}$$

$$(F_{zL} - F_{zR})\frac{y_{eje}}{2} = m_{t-AGV} * g * y_{CM} \tag{21}$$

$$F_{zL} = F_{zFL} + F_{zBL} \tag{22}$$

$$F_{zF} = F_{zFL} + F_{zFR} \tag{23}$$

$$F_{zR} = F_{zFR} + F_{zBR} \tag{24}$$

$$F_{zB} = F_{zBL} + F_{zBR} \tag{25}$$

$$F_Z = F_{zB} + F_{zF} \tag{26}$$

$$F_Z = F_{zL} + F_{zR} \tag{27}$$

where m_{t-AGV} is the mass of the AGV plus the loads carried on it. When referring to a trailer m_{t-AGV} must be replaced by the mass of the trailer and its payload. The terms F_{zij} for $i = \{F,\ B\}$ and $j = \{L,\ R\}$ are the normal forces on the wheels. The subindex i indicates the axle, front "F" or back "B", and the subindex j means the side, left "L" or right "R".

Equations (22)–(25) have been derived from the existing geometry of the wheel distribution in the AGV. This makes it possible to integrate the action of the normal forces on each wheel into a single force that is applied to the axle (front F_{zF} or back F_{zB}) or to the left F_{zL} or right F_{zR} side. The presented solution can be understood as the decomposition of three problems: the balance of momentums in the y-axis direction (20), the balance of momentums in the x-axis direction (21), and the balance of forces (19). From (19), (20), and (26) F_{zB} and F_{zF} are obtained. In addition, from (19), (21), and (27) F_{zL} and F_{zR} are obtained. Then, these values can be used to calculate the four forces in (22)–(25).

The loads on the wheels remain constant during the movement of the AGV as long as the position of the CM does not change. This condition is met for the purposes of this work. By the superposition theorem, these loads can be calculated at the beginning of the simulation, and later the dynamic effects are added to them.

4.5.2. AGV in Motion

When the AGV moves, acceleration and braking forces come into play, as well as centrifugal forces, which modify the load distribution calculated in the previous section. Following the principle of superposition, these forces can be obtained separately and then their effect added to those of the static case.

Centrifugal force is always applied to the center of mass. Acceleration and braking forces, called traction forces, are applied to the center of traction (CT). This point also coincides with the point on which the traction unit pivots. These forces are considered to be the only external forces applied. Figure 13 represents both points of application of the forces.

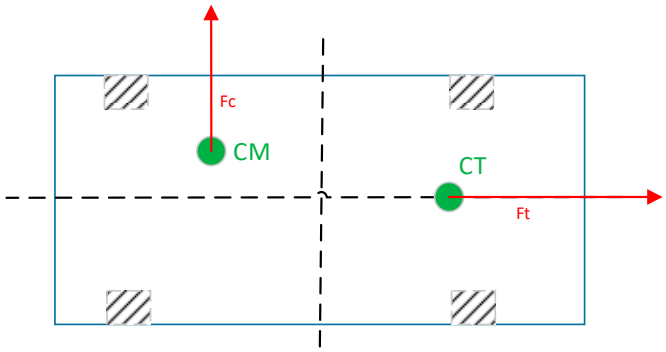

Figure 13. Center of mass and center of traction. Straight movement.

The CT should be located on the x-axis of symmetry of the AGV, otherwise undesired rotational momentum would be generated when applying the pulling force. This consideration allows for a simplification of the calculations, as it will be shown below. It is important to note that F_t does not always act in the direction of the AGV x-axis, for instance, when the movement does not follow a straight line. Figure 14 shows this case.

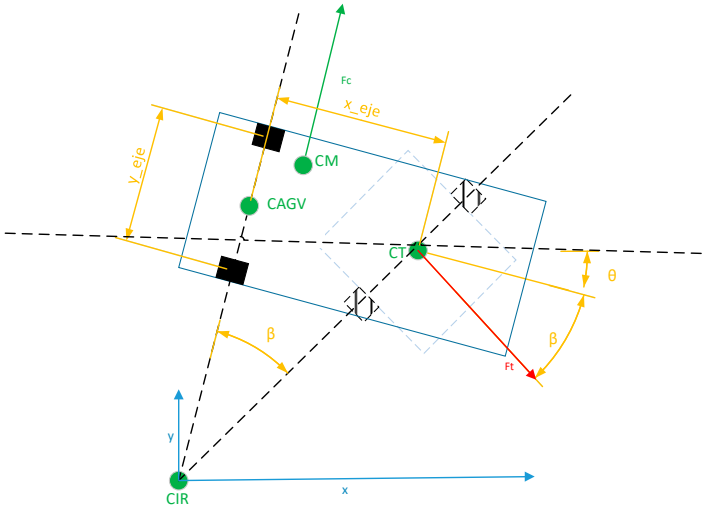

Figure 14. Center of mass and center of traction. Curve movement.

As it can be seen in Figure 14, the wheels of the traction unit are no longer perfectly aligned, as in the previous case. This result is especially relevant when the load is distributed between the four wheels. However, in our case, the drive unit is independent, and the body of the AGV can be modeled as a tricycle. Therefore, the load supported by the front axle is equally distributed between the wheels of the traction unit. This allows the calculations to be greatly simplified.

Figures 15 and 16 represent the action of the tensile and centrifugal forces in the XZ and YZ planes, respectively. It is noteworthy to remember that the action of the weight is not represented as it has been considered in the static case.

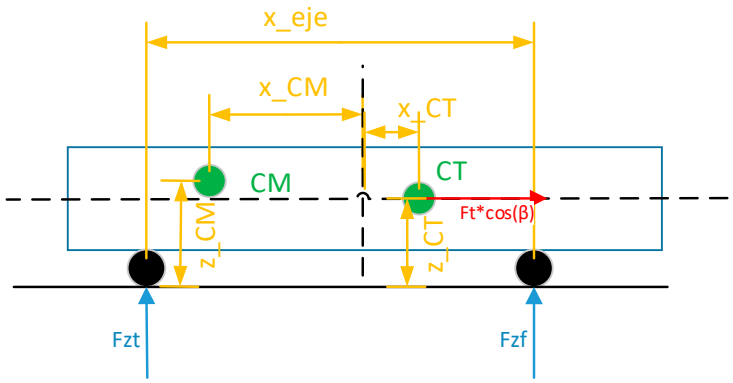

Figure 15. Calculation of the loads on the wheels in motion. XZ plane.

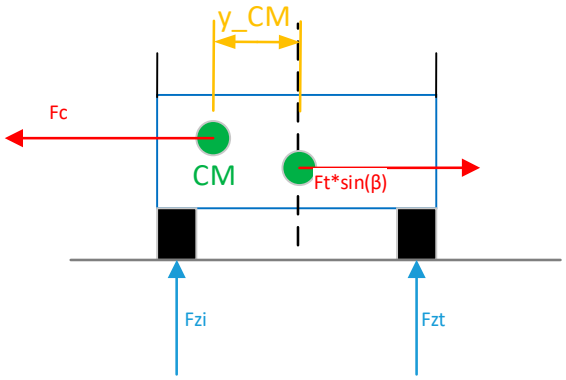

Figure 16. Calculation of the loads on the wheels in motion. YZ plane.

Applying balance of forces and moments with respect to the geometric center of the AGV, the following equations are obtained (28)–(31).

$$F_{zB} = -F_{zF} \tag{28}$$

$$F_t \cos(\beta) z_{CT} = F_{zF} \frac{x_{eje}}{2} \tag{29}$$

$$F_{zL} = -F_{zR} \tag{30}$$

$$F_{zL} \frac{y_{eje}}{2} = F_c z_{CM} \tag{31}$$

where F_{zL}, F_{zR}, F_{zB}, and F_{zF} are defined in the same way as for the static case.

4.6. Lateral Loads on Wheels

When the AGV turns, generated forces tend to make the AGV leave the curve. They must be compensated by the friction between the wheels and the ground so that the AGV turns in a controlled way and follows the desired trajectory.

The main forces to be considered in these cases are the traction force and the centrifugal force. We consider the former applied to the center of traction (CT), while the centrifugal force is applied to the center of mass (CM) of the AGV.

Figure 17 shows both the aforementioned forces and their points of application to the AGV. This section will not go into detail about the calculation of the centrifugal force. It is assumed that the drive unit acts as a single wheel, so that no distinction is made between right and left when calculating the forces applied to the front wheels. Furthermore, it is assumed that the AGV is taking the curve at a constant speed without linear acceleration. The reason for this is to isolate the reactions in the AGV y-axis, which do not contribute to the longitudinal movement of the AGV, from the tractive force, which does contribute.

Therefore, the tractive force does not have to be compensated by the wheels as it generates a net momentum of rotation.

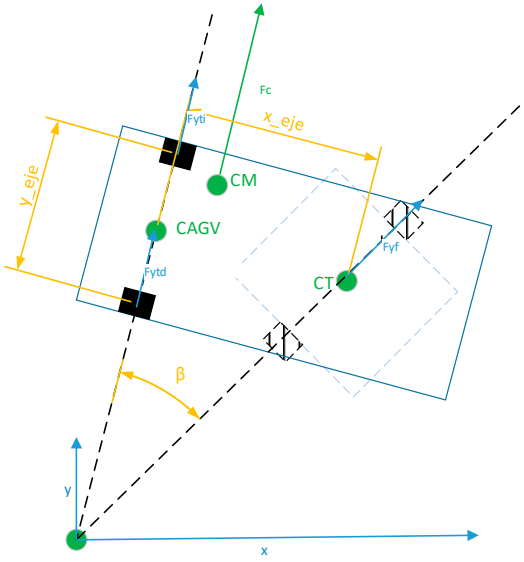

Figure 17. Model of the lateral loads on the wheels.

Another consideration is that the centrifugal force is applied in the direction of the line that joins the CM with the CIR. This implies that it suffers a deviation from the AGV y-axis that varies as a function of the CM x-coordinate. This variation is represented in Figure 18 by the angle α.

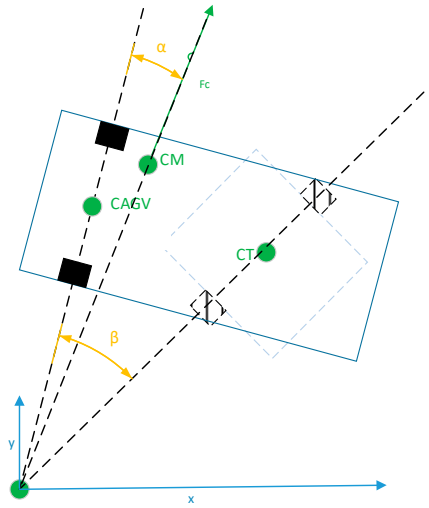

Figure 18. Direction of application of centrifugal force (angle α).

Applying the balance of forces in the AGV x and y directions, and momentum around the geometric center of the AGV, the following equations are obtained (32)–(35):

$$F_{yB} + F_{yF}\cos(\beta) + F_C\cos(\alpha) = 0 \tag{32}$$

$$F_{yF}\sin(\beta) + F_C\sin(\alpha) = 0 \tag{33}$$

$$F_C\sin(\alpha) * y_{CM} + F_c\cos(\alpha) * x_{CM} + F_{yt} * x_{CAGV} + F_{yf}\cos(\beta) * x_{CT} = 0 \tag{34}$$

$$F_{yB} = F_{yBL} + F_{yBR} \tag{35}$$

4.7. Wheel-Ground Interaction Modelling

Once the lateral and vertical forces are obtained, the dynamic model of the AGV must include the wheel-ground interaction to address critical operating conditions. When the AGV is turning, in addition to the traction force, lateral forces are produced. Thus far, it has been assumed that the wheels are capable of compensating for these lateral forces as long as the critical skid conditions are not reached without undergoing any deformation. This hypothesis is an approximation and is not fulfilled under the operating limit conditions.

Wheels suffer deformations that lead to longitudinal and lateral slipping. These displacements depend on the supported vertical load and the lateral stress applied to the wheel. To take this into account, in this work the magic formula is simplified [37], considering only the linear part and then saturating the maximum slip. This implies that the relationship between slip and lateral load supported is given by (36).

$$s_x = K\left(\frac{1}{F_z}\right) * F_x = k_1 * \frac{F_x}{F_z} \tag{36}$$

Therefore, not all the torque transmitted by the wheel motors is used to move the AGV. Part of it is lost in the wheel sliding with respect to the ground.

A similar result can be drawn for the lateral force (37).

$$s_y = K\left(\frac{1}{F_z}\right) * F_y = k_2 * \frac{F_y}{F_z} \tag{37}$$

It can be seen that the wheel slip increases as the lateral load increases and the vertical load decreases. The slip (either longitudinal, s_x, or lateral s_y) can be defined as the ratio of the actual displacement (either longitudinal, Δx, or lateral Δy) to the displacement if the rolling was perfect, Δx_0. These ratios are formalized by:

$$s_x = \frac{\Delta x}{\Delta x_0}, s_y = \frac{\Delta y}{\Delta x_0} \tag{38}$$

The wheels undergo a total slip, which is the sum of the slides on the x (longitudinal) and y (lateral) axes, that is, considering the vertical and lateral loads explained in the previous subsections. The slip of each AGV wheel must be of the same magnitude, otherwise, the AGV would deform.

Automotive data have been used to estimate the constants k1 and k2 [38] of Equations (35) and (36). The values obtained are k1 = 0.006 and k2 = 0.075.

A parameter that could also be considered is the drift angle. It is defined as the angle between the path defined by the AGV and the path it would define in the event that the lateral slides were zero.

$$\delta = \operatorname{atan}\left(\frac{\Delta y}{1 - \Delta x}\right) \approx \frac{\Delta y}{1 - \Delta x} \tag{39}$$

The slide explained in this section must not be mixed up with the slipping of the AGV that must be avoided. Slipping limits are studied in Section 4.3.

5. Model Simulation Results

The algorithm that models the AGV was implemented in Matlab 2016b and was simulated using a discrete step integration in a computer with a processor intel Core i7 with 16 GB of RAM and Windows 10. In the following sub-sections, simulations of the model under different scenarios are presented and discussed.

To study the movement of the AGV, a circular trajectory, a square, and a s-shaped curve were used. Figure 19 (left) shows the test circular trajectory. The path has a circumference centered at (0, 10) and a radius of 10 m. Straight trajectories have been tested during development but are not included here. The AGV system parameters used during the simulations are summarized in Table 3.

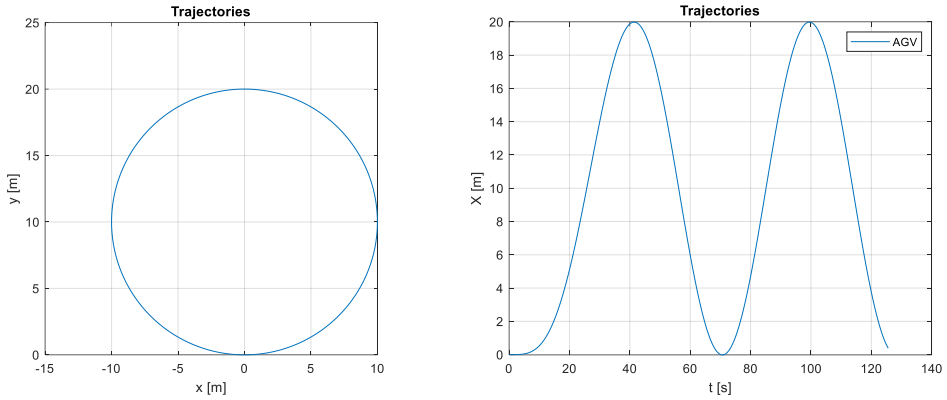

Figure 19. Test trajectory (**left**) and x-axis motion of the AGV without trailers (**right**).

Table 3. AGV system parameters.

Name	Value
m_i	50 kg
CM_i	(0, 0, 0.18) m
CT	(0.2, 0, 0.4) m
B_{UT}	52 cm
L_{UT}	40 cm
B	110 cm
L	40 cm

5.1. AGV with Trailers and without Trailers

First, the movement of the AGV is tested without trailers. Figure 19 (right) shows the evolution over time of the x-axis coordinate of the position of the AGV during two laps of the circuit. The initial position and attitude angle are $(x_0, y_0, \theta_0) = (0, 0, 0)$. As expected, this line has a sinusoidal shape.

Now, the model of the system with nine trailers linked to the AGV is studied. Figure 20 (left) shows the trajectory followed by the AGV and the trailers. The number indicates the order of the trailer, where 1 is the AGV, and 2 is the first trailer, and so on.

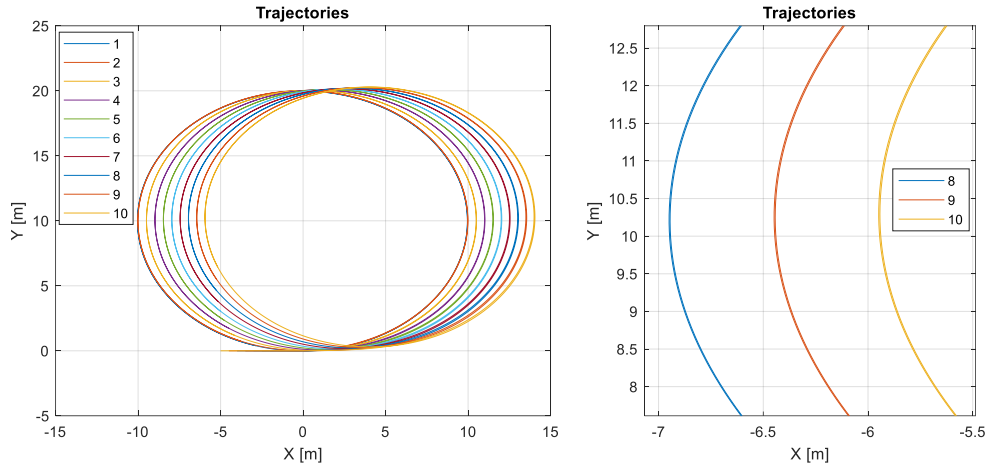

Figure 20. Trajectory followed by the AGV and the trailers (**left**) and a zoomed-in version of the three last trailers (**right**).

When adding trailers to the AGV, it is possible to observe how the trajectories separate from the target as the distance to the tractor unit increases. Thus, the last trailer has the biggest error when following the desired trajectory. In order to better appreciate this, a zoomed-in version of the left part of the trajectory of the last three trailers is shown in Figure 20 (right). The left edge of the trajectory should be -10 in the x-axis, but it is between -7.2 and 6 for these trailers. The distance to -10 grows with the number of trailers.

Figure 21 shows the x-coordinate of the position of the AGV and the trailers during the first two laps. The legend is the same as in Figure 20. This figure allows us to better see the differences among trailers. First, it is noticeable how the trailers describe a more open turn than the AGV unit. In addition, the x-axis component of the trajectory of all trailers describes a sinusoidal signal with similar amplitude and frequency. However, they present an offset and delay that grow with an increasing distance from the trailer to the AGV. This results in a larger error with respect to the reference path.

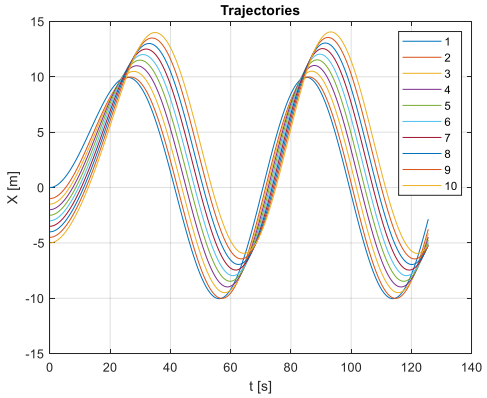

Figure 21. Position of the AGV and the trailers in the x-coordinate for the circumference trajectory.

Figure 22 shows the trajectory described by the AGV and the trailers when the AGV follows a square (left) and an s-shaped curve (right). The number indicates the order of the trailer, where 1 is the AGV, 2 is the first trailer, and so on. In the case of the square, the initial position and attitude angle are $(x_0,\ y_0,\ \theta_0) = (0,\ 0,\ 0)$. In turn, the initial position and attitude angle for the s-shaped curve are $(x_0,\ y_0,\ \theta_0) = (0,\ 0,\ \pi/2)$. As expected, it is possible to observe how the error grows as the trailer moves farther away.

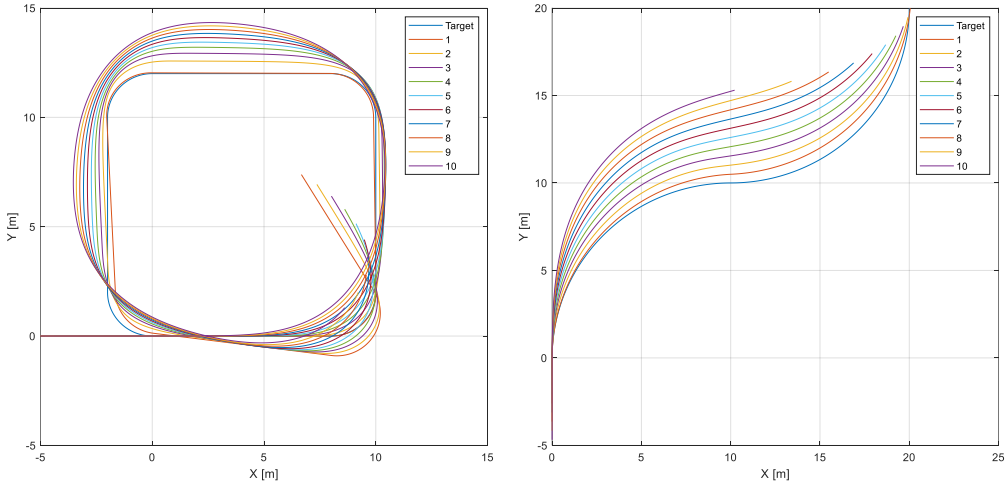

Figure 22. Trajectory followed by the AGV and the trailers when the reference is a square (**left**) and an s-shaped curve (**right**).

5.2. Sped Tracking

In this experiment, the speed reference is a sinusoidal signal with a 0.5 m/s amplitude and an average value of 0.5 m/s, and the trajectory is the s-shaped curve. The double PID and the PID-FLC controller (Figures 4 and 5) have been tested. Figure 23 shows in blue the target speed, in red the speed obtained when the PID speed controller is used, and in yellow the FLC. Both controllers provide similar responses, although the FLC is a little faster.

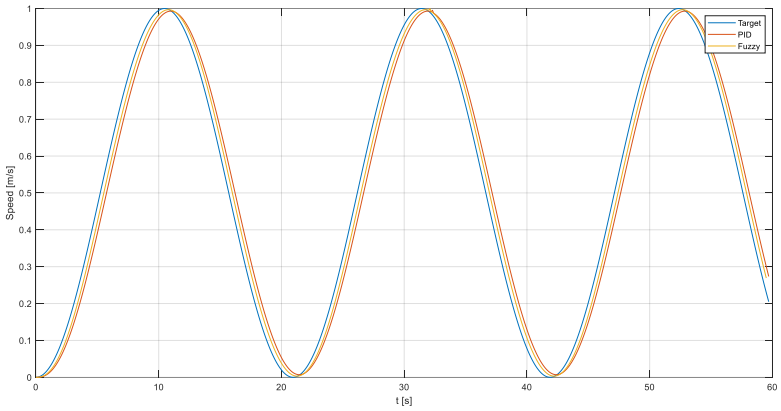

Figure 23. Comparison of speed tracking provided by a PLC and a FLC controller.

Figure 24 shows the tracking of the s-shaped trajectory for both controllers. As expected, as the speed controllers work well, the tracking of the trajectory is not affected. Thus, it is noticeable how both controllers provide a good tracking performance.

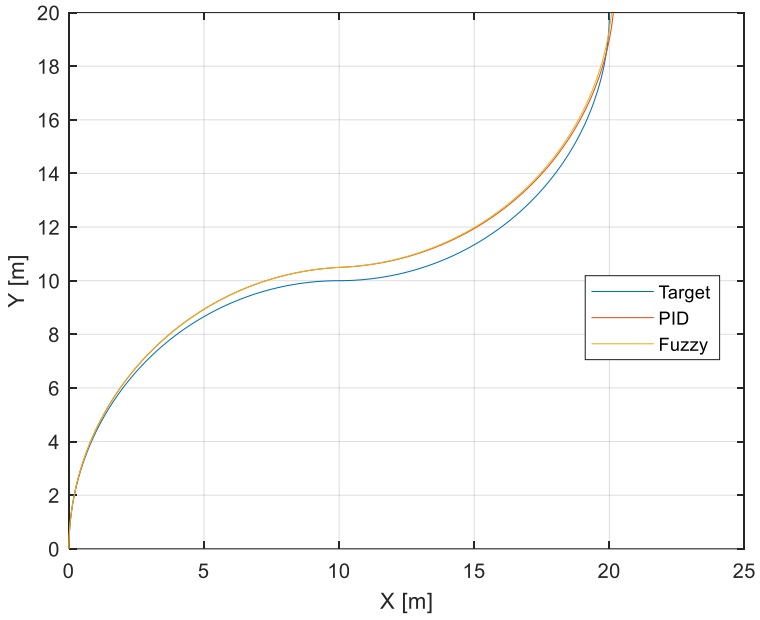

Figure 24. Comparison of the tracking of the s-shaped curve for both controllers.

5.3. Including Disturbances in the Model

Table 2 summarizes the main uncertainties and disturbances that can appear in the AGV model. In this experiment, we have studied what happens when there is a disturbance in the lateral friction. Results are shown in Figure 25. The x and y coordinates of the AGV and the trailer are shown on the left figure. The figure on the right shows the time evolution of the signals.

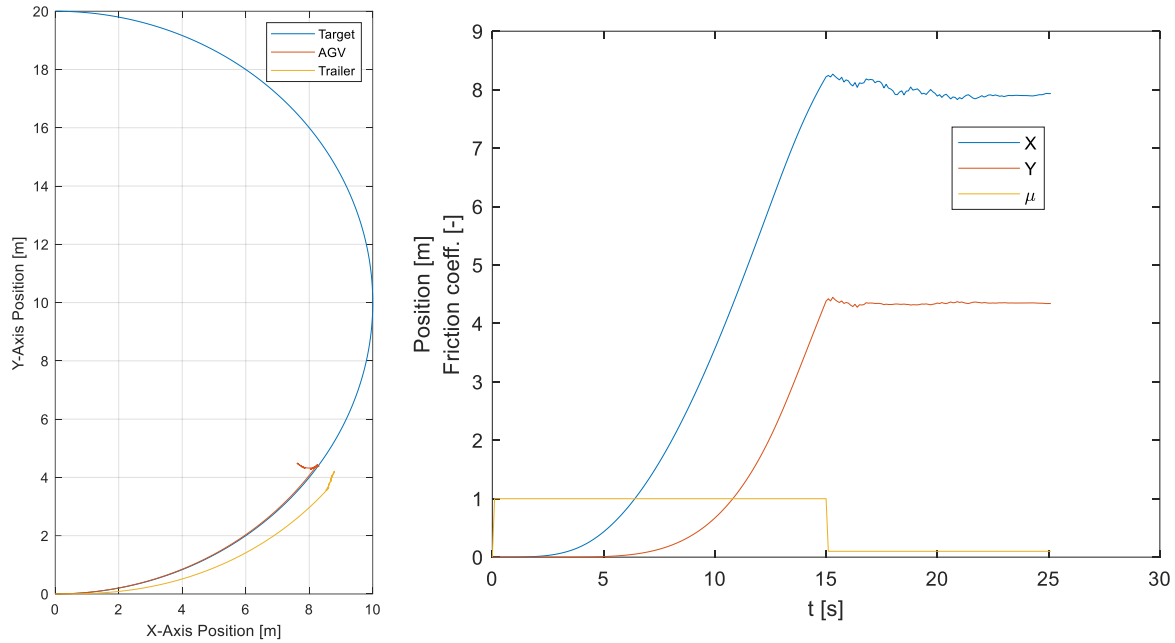

Figure 25. Trajectory followed by the AGV and the trailer with an abrupt change in the lateral friction.

It is possible to observe how the lateral friction suffers a marked decrement around t = 15 s. Before this time, the AGV correctly followed the circular trajectory. However, when the lateral friction decreases, the AGV skids, hence producing a tracking error.

5.4. Influence of the Number of Trailers on the Controller Performance

In order to study the influence of the number of trailers on the controller's performance, different simulations have been carried out, changing the number of trailers. For each simulation, the mean squared error (MSE) of the guiding error (40) and the control effort (41) have been evaluated. It is important to reduce both metrics. Maintaining a low guiding error is key to ensuring correct positioning of the AGV and trailers in the work stations, to pick up and leave the parts, as well as to ensure a correct charging operation. On the other hand, the reduction in the control effort is necessary for avoiding degradation in its mechanical components and extending its life.

These metrics have been calculated using Equations (40) and (41).

$$MSE = \frac{1}{T_{sim}} \sum err_{gui}(t_i) \tag{40}$$

$$CE = \frac{1}{T_{sim}} \sum F_L(t_i)^2 + F_R(t_i)^2 \tag{41}$$

Figure 26 shows the growth of the MSE of the guiding error with the number of trailers. This guiding error is the error experienced after the traction unit of the AGV follows the pre-defined trajectory. This must not be mixed up with the error of each trailer commented in the previous sub-section. It is possible to see how the use of only one trailer hardly affects the error (the MSE value for zero trailers and one trailer is similar). However, when there is more than one trailer, the error grows, but not in a regular way. The differential increment is bigger at the beginning (from number 2 on), and it gets smaller and smaller up to a constant value (from 10 trailers on). It should be noted that this number cannot be increased indefinably, there exists a maximum number of trailers that depends on the maximum torque, the total payload, and the friction coefficient.

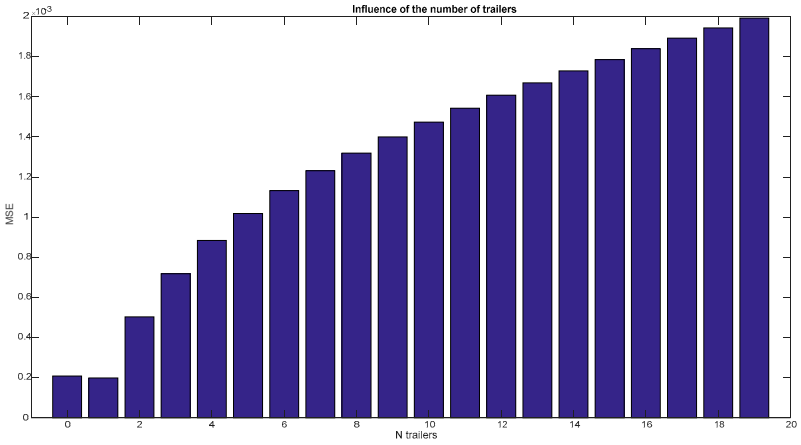

Figure 26. Influence of the number of trailers in the guiding error.

The effect of the number of trailers in the control effort is represented in Figure 27. In this case, it increases monotonically with the number of trailers. Curiously, as in Figure 26, the first trailer does not seem to affect the metric.

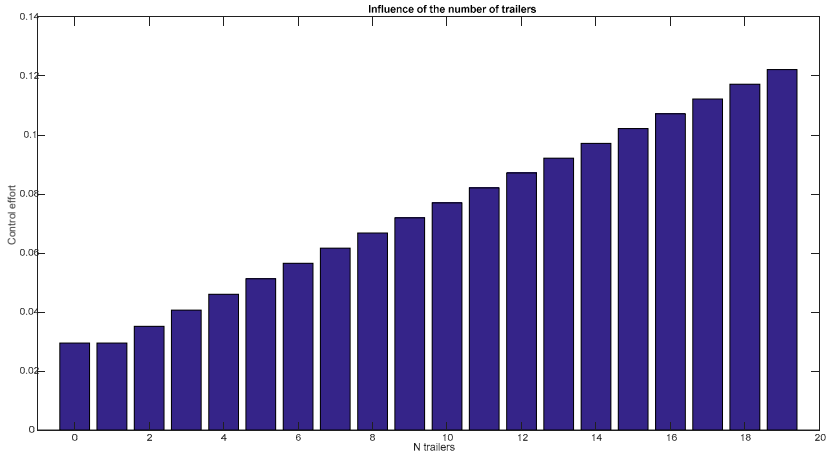

Figure 27. Influence of the number of trailers in the control effort.

5.5. Slipping Limit

Lateral slipping occurs when the frictional force is not enough to compensate the centrifugal force (42).

$$m_t \frac{V_d^2}{R} > \mu \cdot g \cdot m_t \tag{42}$$

where R is the radius of the plotted curve and μ is the friction coefficient. Based on this equation, it is easy to find a limit speed to avoid lateral slipping (43).

$$V_d < \sqrt{gR\mu} \tag{43}$$

In Figure 28, the variation of the limit speed with the curve radius for different friction coefficients is represented. Considering these results, it can be concluded that for these friction coefficients the model of AGV used in this study would never skid since its maximum speed is 1 m s and its minimum turning radius is 1 m.

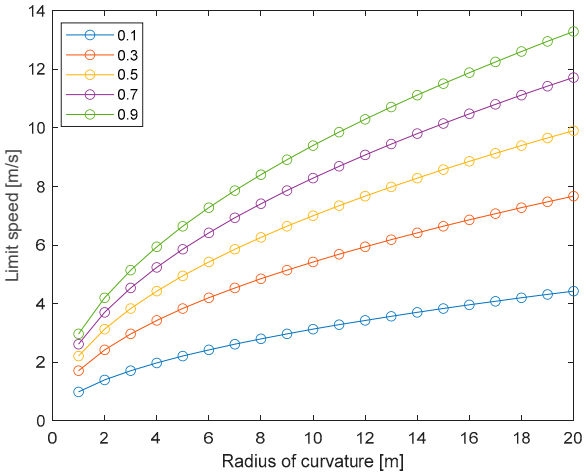

Figure 28. Lateral slipping limit speed.

By manipulating Equation (43), it is also possible to obtain the critical friction coefficient, that is, the minimum friction coefficient to guarantee there is no lateral slipping (44). If we consider R_{min} = 1 m and V_{max} = 1 m/s, thus:

$$\mu_{crit} = \frac{V_{max}^2}{gR_{min}} \approx \frac{1}{g} \approx 0.1 \tag{44}$$

It is important to emphasize that these equations assume that the load is symmetrically distributed between all axes of the AGV, and thus the center of gravity is centered. The effect of a different load distribution is analyzed in the next sub-section.

In addition, despite how unlikely the slipping of the whole AGV is, the slippage of the load is a different situation. If the load is big and not properly secured on the AGV, it could shift or even come off when turning. To avoid this dangerous situation, the same critical coefficient of friction (44) must be applied to load-load surface contact.

5.6. Capsizing Limit

In order to study the capsizing conditions, it is interesting to show the forces from a frontal view of the AGV (Figure 29).

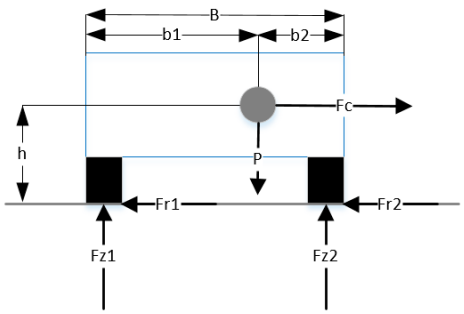

Figure 29. Application of centrifugal force. Frontal view.

The application of the balance of the torques on the center of gravity results in (45),

$$Fz_2 b_2 - Fz_1(B - b_2) = (Fr_1 + Fr_2)h \tag{45}$$

Considering that $Fz_1 + Fz_2 = mg$ and $Fr_1 + Fr_2 = F_c$, it is possible to obtain the value of Fz_1,

$$Fz_1 = \frac{m_t g b_2}{B} - \frac{m_t {V_d}^2 h}{R \cdot B} \tag{46}$$

Rollover occurs when the value of Fz_1 becomes negative. Thus, by rewriting expression (46) it is possible to obtain the condition to avoid rollover (47).

$$V_v < \sqrt{\frac{gRb_2}{h}} \tag{47}$$

In Figure 30, the evolution of the limit speed with respect to the radius of the curve is represented. To obtain this figure, it has been assumed that the center of gravity is at h = 50 cm and $b_2 = 62$ cm, which corresponds to possible real values. Other assumptions would be possible for different curves.

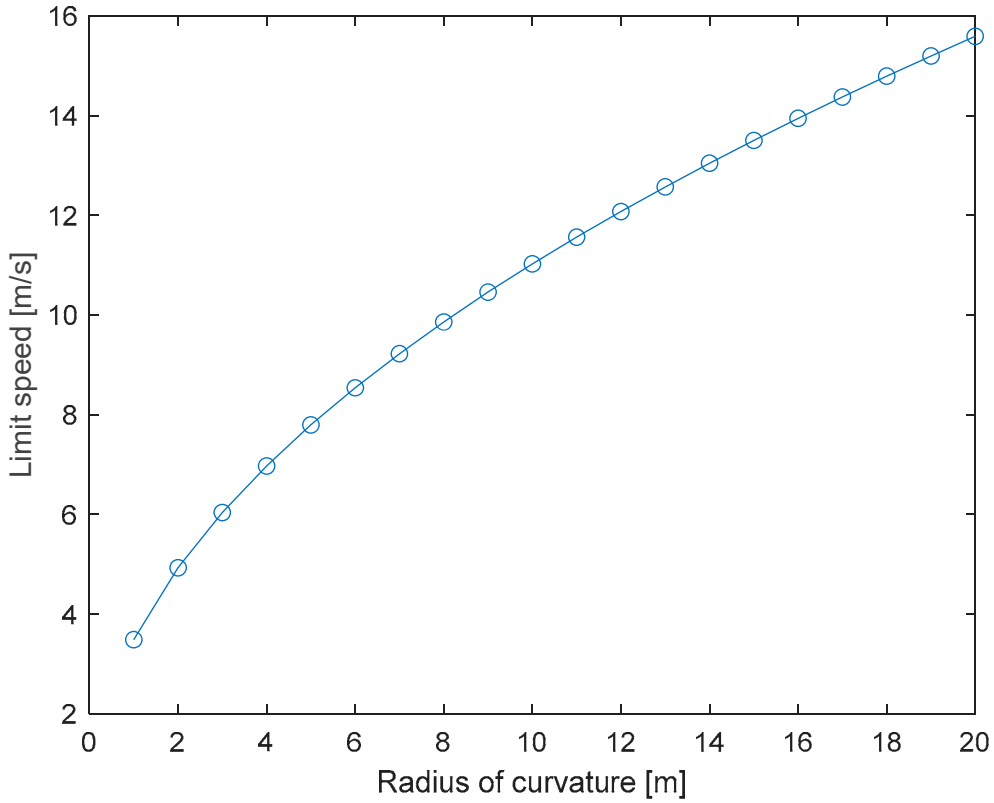

Figure 30. Capsizing speed limit for h = 50 cm and $b_2 = 62$ cm.

If we consider that the turning radius of the AGV used in this work is 1 m and the maximum speed is 1 m/s, we can conclude that the AGV would not capsize under this center of mass distribution. We can define a parameter with the ratio between the lateral and height displacements of the center of gravity, C = b2/h. This way, the parameter represents the relative position of the center of mass.

Based on (47), the critical value of the C parameter is obtained, that is, the minimum value of C that allows the AGV to avoid capsizing. With the AGV data we are working with, the critical value of C is (48).

$$C_{crit} = \frac{V_{max}^2}{gR_{min}} = \frac{1}{g} \approx 0.1 \tag{48}$$

Figure 31 shows the critical values of h and b_2 for which the AGV would tip over under extreme conditions (R = 1 m, V = 1 m/s).

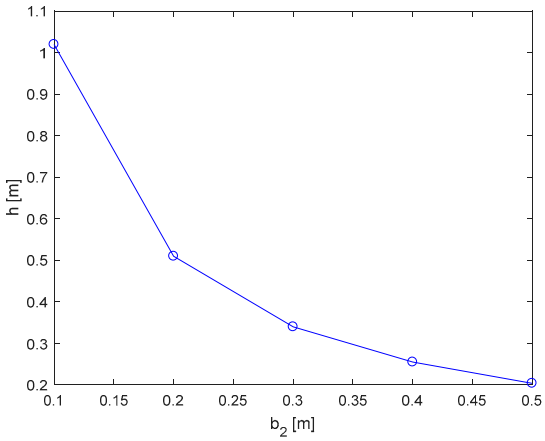

Figure 31. Critical values of height and position of the AGV CM to cause capsizing.

These results help us identify what load distribution causes the AGV to overturn. For the AGV considered in this study, these circumstances occur when the load makes the center of gravity highly foreshortened to one side or at a very large height. Therefore, to maximize stability, one should try to bring the center of mass to a lower and centered position.

6. Conclusions and Future Works

Two AGVs were used in the intra-logistic industrial processes to carry out all types of loads. Unlike the turtle AGVs, they do not have to support the weight of the payload, which in this case is carried by trailers or carts. This fact allows it to move bigger and heavier loads with smaller AGVs and motors and, thus, they have become very popular vehicles in the Industry 4.0 framework. Indeed, several trailers can be simultaneously used to extend the capacity of the mobile robot. For these multi-trailer AGVs, it is of utmost importance to count on computational models in order to analyze their performance and design effective control strategies to provide them with the flexibility required by Industry 4.0.

In this work, a hybrid (tricycle-differential) multi-trailer AGV modeling iterative algorithm is proposed. The developed mathematical model considers the dynamics of the components of the mobile robot traction unit, body, trailer, with the vertical and lateral loads, and the effect of wheel deformation due to interaction with the ground. To obtain the model, the Newton–Euler equations were iteratively applied to all subsystems of the AGV. Then the traction force of the AGV unit is calculated and applied to obtain the movement of the whole vehicle. In turn, this movement is transformed into a traction force to provide the trailer's motion.

The model has been validated through simulation and the effects of the payload, number of trailers, weight distribution, as well as critical circumstances of slippage and capsizing analyzed. The outcomes are realistic, and they enable the design of the controls and safety conditions to operate more effectively.

In future work, we may highlight the integration of the electrical equations of the motors in the model, the development of more sophisticated controllers for these mechanical systems, and the estimation of the degradation of the mechanical components.

Author Contributions: Conceptualization, R.S.-M., J.E.S.-G., and M.S.; methodology, R.S.-M., J.E.S.-G., and M.S.; software, R.S.-M.; validation, R.S.-M., J.E.S.-G., and M.S.; formal analysis, R.S.-M., J.E.S.-G., and M.S.; investigation, R.S.-M., J.E.S.-G., and M.S.; resources, R.S.-M., J.E.S.-G., and M.S.; data curation, R.S.-M., J.E.S.-G., and M.S.; writing—original draft preparation, R.S.-M., J.E.S.-G., and M.S.; writing—review and editing, R.S.-M., J.E.S.-G., and M.S.; visualization, R.S.-M., J.E.S.-G., and M.S.; supervision, J.E.S.-G. and M.S.; project administration, J.E.S.-G. and M.S. All authors have read and agreed to the published version of the manuscript.

Funding: This research received no external funding.

Data Availability Statement: Data are available under request.

Conflicts of Interest: The authors declare no conflict of interest.

Abbreviations

β	Turning angle of the tractor head with respect to the body of the AGV [rad]
B_{UT}	Traction unit wheelbase [m]
L_{UT}	Traction unit length [m]
ω_{UT}	Traction unit rotation speed [rad/s]
F_{TR}, F_{TL}	Traction force of each wheel [N]
Fx_UT, Fy_UT	Resulting forces at the center of traction [N]
M_UT	Resulting moment at the center of traction (it allows the traction unit and, hence, the AGV, to rotate) [Nm]
CT	Center of traction
Fc_UT	Centrifugal force acting on the traction unit [N]
mAGV*aAGV	Force exerted by the body of the AGV on the traction unit [N]

References

1. Zamora-Cadenas, L.; Velez, I.; Sierra-Garcia, J.E. UWB-Based Safety System for Autonomous Guided Vehicles without Hardware on the Infrastructure. *IEEE Access* **2021**, *9*, 96430–96443. [CrossRef]
2. Espinosa, F.; Santos, C.; Sierra-García, J.E. Multi-AGV transport of a load: State of art and centralized proposal. *Rev. Iberoam. Autom. Inf. Ind.* **2020**, *18*, 82–91. [CrossRef]
3. Abderrahim, M.; Bekrar, A.; Trentesaux, D.; Aissani, N.; Bouamrane, K. Manufacturing 4.0 Operations Scheduling with AGV Battery Management Constraints. *Energies* **2020**, *13*, 4948. [CrossRef]
4. Dintén, R.; López Martínez, P.; Zorrilla, M. Reference architecture for the design and development of applications for Industry 4.0. *Rev. Iberoam. Autom. Inf. Ind.* **2021**, *18*, 300–311. [CrossRef]
5. Aloui, K.; Hammadi, M.; Guizani, A.; Soriano, T.; Haddar, M. Development of an AGV system using MBSE method and multi-agents' technology. In Proceedings of the 9th Conference on Design and Modeling of Mechanical Systems, Hammamet, Tunisia, 20–22 December 2021; pp. 103–114.
6. Li, G.; Lin, R.; Li, M.; Sun, R.; Piao, S. A master-slave separate parallel intelligent mobile robot used for autonomous pallet transportation. *Appl. Sci.* **2019**, *9*, 368. [CrossRef]
7. Belman-López, C.E.; Jiménez-García, J.A.; Hernández-González, S. Análisis exhaustivo de los principios de diseño en el contexto de Industria 4.0. *Rev. Iberoam. Autom. Inf. Ind.* **2020**, *17*, 432–447. [CrossRef]
8. Niestrój, R.; Rogala, T.; Skarka, W. An Energy Consumption Model for Designing an AGV Energy Storage System with a PEMFC Stack. *Energies* **2020**, *13*, 3435. [CrossRef]
9. López, J.; Zalama, E.; Gómez-García-Bermejo, J. A simulation and control framework for AGV based transport systems. *Simul. Model. Pract. Theory* **2022**, *116*, 102430. [CrossRef]
10. Dobrzanska, M.; Dobrzanski, P. Simulation modelling of material handling using AGV. *IOP Conf. Ser. Mater. Sci. Eng.* **2021**, *1199*, 012015. [CrossRef]
11. Mahulea, C.; González, R.; Montijano, E.; Silva, M. Path planning of multirobot systems using Petri net models. Results and open problems. *Rev. Iberoam. Autom. Inf. Ind.* **2021**, *18*, 19–31. [CrossRef]
12. Sierra, J.E.; Santos, M. Modelling engineering systems using analytical and neural techniques: Hybridization. *Neurocomputing* **2018**, *271*, 70–83. [CrossRef]
13. Bonilla, I.; Reyes, F.; Mendoza, M. Modelling and simulation of a wheeled mobile robot in configuration classical tricycle. In Proceedings of the 5th WSEAS International Conference on Instrumentation, Measurement, Control, Circuits and Systems, Cancún, Mexico, 11–14 May 2005.
14. Yun, D.U. Kinematics and Dynamic Modeling and Simulation Analysis of Three-wheeled Mobile Robot. In Proceedings of the 2016 MDM International Conference on Mechanics Design, Manufacturing and Automation, Catania, Italy, 14–16 September 2016.
15. Bi, Z.M.; Lang, S.Y.; Wang, L. Improved control and simulation models of a tricycle collaborative robot. *J. Intell. Manuf.* **2008**, *19*, 715–722. [CrossRef]
16. Montazerijouybari, M.; Baron, L.; Kelouwani, S. Kinematics of 2-DOF AGVs with Differential Driving Wheels and Caster Wheels Modeling. In *Symposium on Robot Design, Dynamics and Control*; Springer: Berlin/Heidelberg, Germany, 2020; pp. 495–502.
17. Villagra, J.; Herrero-Pérez, D. A comparison of control techniques for robust docking maneuvers of an AGV. *IEEE Trans. Control Syst. Technol.* **2011**, *20*, 1116–1123. [CrossRef]
18. Suárez, J.I.; Vinagre, B.M.; Gutiérrez, F.; Naranjo, J.E.; Chen, Y.Q. Dynamics models of an AGV Based on Experimental Results. In Proceedings of the 5th IFAC Symposium on Intelligent Autonomous Vehicles, Lisbon, Portugal, 5–7 July 2004.
19. Rahimi, A.; He, Y. A review of essential technologies for autonomous and semi-autonomous articulated heavy vehicles. In Proceedings of the Canadian Society for Mechanical Engineering International Congress 2020, Charlottetown, PE, Canada, 21–24 June 2020; pp. 21–24.

20. Rahimi, A.; Huang, W.; Sharma, T.; He, Y. An autonomous driving control strategy for multi-trailer articulated heavy vehicles with enhanced active trailer safety. In *The IAVSD International Symposium on Dynamics of Vehicles on Roads and Tracks*; Springer: Berlin/Heidelberg, Germany, 2022; pp. 769–782.
21. Deng, Z.W.; Zhao, Q.X.; Zhao, Y.Q.; Wang, B.H.; Gao, W.; Kong, X.X. Active LQR Multi-Axle-Steering Method for Improving Maneuverability and Stability of Multi-Trailer Articulated Heavy Vehicles. *Int. J. Automot. Technol.* **2022**, *23*, 939–955. [CrossRef]
22. Zhou, X.; Jin, L.; Liu, Y. Modeling and Simulation Research of Heavy-duty AGV Tracking Control System Based on Magnetic Navigation. *J. Phys. Conf. Ser.* **2021**, *1746*, 012021. [CrossRef]
23. Islam, M.M.; He, I. A parallel design optimisation method for articulated heavy vehicles with active safety systems. *Int. J. Heavy Veh. Syst.* **2013**, *20*, 327–341. [CrossRef]
24. Islam, M.M.; Ding, X.; He, Y. A closed-loop dynamic simulation-based design method for articulated heavy vehicles with active trailer steering systems. *Vehicle Syst. Dyn.* **2012**, *50*, 675–697. [CrossRef]
25. Govender, T. Design and Analysis of a Multi-Trailer System for the Durban Container Terminal. Ph.D. Thesis, University of KwaZulu-Natali, Durban, South Africa, 2018.
26. Ottjes, J.A.; Duinkerken, M.B.; Evers, J.J.; Dekker, R. Robotised inter terminal transport of containers. In Proceedings of the 8th European Simulation Symposium, Genoa, Italy, 24–26 October 1996; pp. 621–625.
27. Veiga, J.; Sousa, J.; Machado, J.; Mendonça, J.; Machado, T.; Silva, P. Modeling of Dynamic Behavior of AGV systems. In Proceedings of the 2019 6th International Conference on Control, Decision and Information Technologies (CoDIT), Paris, France, 23–26 April 2019; pp. 1307–1312.
28. Jodejko-Pietruczuk, A.; Werbińska-Wojciechowska, S. Availability assessment for a multi-AGV system based on simulation modeling approach. In Proceedings of the 2021 International Conference on Electrical, Computer, Communications and Mechatronics Engineering (ICECCME), Mauritius, Mauritius, 7–8 October 2021; pp. 1–6.
29. Sasamoto, H.; Velázquez, R.; Gutiérrez, S.; Cardona, M.; Ghavifekr, A.A.; Visconti, P. Modeling and Prototype Implementation of an Automated Guided Vehicle for Smart Factories. In Proceedings of the 2021 IEEE International Conference on Machine Learning and Applied Network Technologies (ICMLANT), Soyapango, El Salvador, 16–17 December 2021; pp. 1–6.
30. Smieszek, M.; Dobrzanska, M.; Dobrzanski, P. The impact of load on the wheel rolling radius and slip in a small mobile platform. *Auton. Robot.* **2019**, *43*, 2095–2109. [CrossRef]
31. Reis, W.P.N.D.; Couto, G.E.; Junior, O.M. Automated guided vehicles position control: A systematic literature review. *J. Intell. Manuf.* **2022**, 1–63. [CrossRef]
32. Molledo, V.R.; Garcia, J.E.S. Simulation Tool for Hybrid AGVs based on IEC-61131. *IEEE Lat. Am. Trans.* **2021**, *20*, 317–325. [CrossRef]
33. Moshayedi, A.J.; Li, J.; Sina, N.; Chen, X.; Liao, L.; Gheisari, M.; Xie, X. Simulation and Validation of Optimized PID Controller in AGV (Automated Guided Vehicles) Model Using PSO and BAS Algorithms. *Comput. Intell. Neurosci.* **2022**, *2022*, 7799654. [CrossRef] [PubMed]
34. Kim, D.H.; Kim, S.B. Path following control of automated guide vehicle using camera sensor. In *International Conference on Advanced Engineering Theory and Applications*; Springer: Berlin/Heidelberg, Germany, 2018; pp. 932–938.
35. AGVExpertJS. Tugger AGV Towing Multiple Trailers in a Warehouse. Environment. 2022. Available online: https://en.wikipedia.org/wiki/Automated_guided_vehicle#/media/File:Tugger_AGV_with_trailers,_courtesy_of_Egemin_Automation_Inc.jpg (accessed on 24 August 2022).
36. Sierra-Garcia, J.E.; Santos, M. Combining reinforcement learning and conventional control to improve automatic guided vehicles tracking of complex trajectories. *Expert Syst.* **2022**, e13076. [CrossRef]
37. Han, K.; Choi, M.; Choi, S.B. Estimation of the tire cornering stiffness as a road surface classification indicator using understeering characteristics. *IEEE Trans. Veh. Technol.* **2018**, *67*, 6851–6860. [CrossRef]
38. Aparicio Izquierdo, F.; Vera Alvarez, C.; Díaz López, V. *Teoría de los vehículos automóviles*; Ets Ingenieros Industriales, Universidad Politécnica de Madrid: Madrid, Spain, 1995; ISBN 8474841461.